THE ASTROPHYSICAL JOURNAL, 417:243–258, 1993 November 1

COLLAPSE OF MAGNETIZED MOLECULAR CLOUD CORES. II. NUMERICAL RESULTS

DANIELE GALLI[1] AND FRANK H. SHU[2]
Department of Astronomy, University of California at Berkeley
Received 1993 January 25; accepted 1993 May 10

ABSTRACT

In a previous paper (Paper I) we presented a perturbative analysis of the collapse of a molecular cloud core threaded by an ordered magnetic field, obtaining a semianalytical solution applicable over a moderate range of temporal and spatial scales. In the present paper we supplement this analysis with a numerical solution of the magnetohydrodynamic (MHD) equations that include the effects of ambipolar diffusion, valid in the region where magnetic effects dominate the dynamics of the collapse. We focus on the formation of a flattened disequilibrium structure ("pseudodisk") around the central protostar. The numerical solution gives dimensionless values for the radius of the pseudodisk as a function of time. Combined with the analytical scaling laws found in Paper I, these results provide in the small time limit a simple power-law expression for the dimensional radius of the pseudodisk as a function of the initial magnetic field B_0 and effective sound speed a of the unstable molecular cloud core. We tabulate in nondimensional form the velocity, density, and magnetic fields as functions of the radius, polar angle, and time for two values ($\chi = 11.3$ and ∞) of the ion-neutral coupling constant. We apply the results to the density and magnetic field structures on the astronomically interesting scale of a few hundred to a few thousand AU around protostars with mass in the range 0.57–2.0 $M_\odot$. The resultant magnetic field topology causes us to speculate on the importance of neutral-ion slip, ohmic dissipation, and reconnection in the overall problems of the loss of flux and the isolation of the magnetic fields in the pseudodisk (and smaller centrifugal disk) from their interstellar origins. We conclude by comparing our results with observations of flattened dense structures around young stellar objects in various stages of evolution.

Subject headings: ISM: clouds — ISM: magnetic fields — ISM: molecules — MHD — stars: formation

1. INTRODUCTION

In a previous paper (Galli & Shu 1993, hereafter Paper I) we introduced a strategy for studying the collapse of the magnetic molecular cloud core, dividing the overall problem into distinct regions in which different simplifying assumptions hold to high accuracy. Following this approach, Paper I treated the part of the problem where the dynamical effects of the magnetic field are relatively small (the "intermediate region") by a perturbative attack. The nonmagnetic collapse of the singular isothermal sphere represents a good zeroth-order reference state for the intermediate region, which possesses a known analytical solution (Shu 1977) in terms of the similarity variable $x \equiv r/at$, where a is the effective sound speed, t is the elapsed time since the initiation of dynamical collapse, and r is the radial distance from the center of the forming protostar. Departures introduced by the presence of an initial magnetic field of uniform strength B_0 can be developed as a series expansion in the square of the dimensionless time $\tau \equiv t/t_m$, where $t_m \equiv 2a/G^{1/2}B_0$ with G equal to the universal gravitation constant. The series expansion should converge rapidly for an intermediate range of values of x (defined in Paper I) in the "small-time" limit $\tau^2 \ll 1$. Once the ordering of terms in τ^2 has occurred, we can further simplify by introducing a spectral decomposition of the variations with polar angle θ in terms of (axisymmetric) vector spherical harmonics. We then obtain the radial part of the solution of the coefficients outside of the expansion wave as an analytical infinite series in the inverse of the similarity variable x^{-1} and the coefficients inside the expansion wave via the numerical integration in x of a set of ordinary differential equations (ODEs), with continuity of all physical variables imposed at the head of the expansion wave with unperturbed position at $x = 1$ (see Paper I for details).

Our method easily incorporates the effects ("ambipolar diffusion") of finite slip velocity $(\boldsymbol{u}_n - \boldsymbol{u}_i)$ between ions of a small mass density ρ_i and neutrals of mass density ρ_n. In the special case when the ionization law and the drag force per unit volume read $\rho_i = C\rho_n^{1/2}$ and $\boldsymbol{f}_d = \gamma\rho_i\rho_n(\boldsymbol{u}_i - \boldsymbol{u}_n)$, the effects are entirely contained in a dimensionless ion-neutral coupling-constant $\chi \equiv \gamma C/(4\pi G)^{1/2}$ (see Paper I). For "standard" values of γ and C, $\chi = 11.3 \gg 1$, and the effects of ambipolar diffusion remain minor until the governing relationships change functional forms. Complications enter when $\rho_n > 10^{-13}$ g cm^{-3} (see, e.g., Nakano & Umebayashi 1986a, b), but such densities greatly exceed the typical values encountered in the regime treated in this paper, so we shall continue to assume that the effects of ambipolar diffusion can be subsumed in a single parameter χ. For numerical work, we shall assume χ to have either the value, 11.3, appropriate for the "standard model," or the value, ∞, appropriate for complete flux freezing. Other choices of χ, as long as $\chi \gg 1$, may be obtained by interpolation or extrapolation in $1/\chi$ from the results for these two cases.

In this paper we wish to study the "inner region" where Lorentz forces dominate the dynamics of the collapse because of the larger compression of the field introduced by conditions for near flux freezing. Matter infalling in the inner region along the polar axis (defined by the direction of the initial magnetic field) lands directly on the central protostar, whereas Lorentz forces deflect falling gas along initially radial streamlines at larger polar angles toward the equatorial plane, forming a flat-

[1] Postal address: Osservatorio Astrofisico di Arcetri, Largo E. Fermi, I-50125 Firenze, Italy.
[2] Postal address: Department of Astronomy, 601 Campbell Hall, University of California, Berkeley, CA 94720.

tened dense structure that we call the *pseudodisk*. The radius t_B of the pseudodisk is defined by the outermost intersection of the ballistic trajectories of electrically conducting fluid elements on (barely) opposite sides of the equatorial plane. The perturbative analysis presented in Paper I gives the scaling of r_B with the physical variables of the problem as

$$r_B = k_B\left(\frac{G^2 B_0^4}{a}\right)^{1/3} t^{7/3} \tag{1}$$

independent of the value of χ (as long as it is large compared to unity), but it does not provide a numerical value for the nondimensional coefficient k_B.

In this paper we determine by numerical computation that $k_B = 0.12$. Moreover, we find in the inner region that Lorentz forces introduce large deviations from the behavior appropriate for the nonmagnetic collapse problem. Because the nonmagnetic solution provides the zeroth-order reference state for the method developed in Paper I, the perturbative technique breaks down inside $x_p \simeq 0.2\tau^{4/3}$ (see § 5.5 of Paper I), and we are led to a numerical solution of the fully nonlinear problem for $x < x_p$.

2. FORMULATION OF THE PROBLEM

2.1. *The Equations for the Inner Region*

We wish to investigate the solution of the two-fluid MHD equations (34)–(38) of Paper I (hereafter eqs. [I.34] and [I.38]) inside a region $x_p \ll 1$ (refer to the Appendix for definitions of dimensionless variables). Since the computational domain constitutes a small fraction of the region encompassed by the expansion wave ($x = 1$), useful approximations exist to reduce the complexity of these equations.

A first simplification results from the gravitational potential of the central mass asymptotically dominating over the gravitational potential of the infalling material for small x. As a consequence Poisson's equation has the approximate solution $\psi(x, \tau) \simeq -m_0/x$, where we may adopt for simplicity $m_0 = m^{(0)}(0) = 0.975$, ignoring the correction in τ^2, which has a very small numerical coefficient according to the results of § 5.4 in Paper I. As a second approximation, the supersonic inflow allows us to neglect the effects of pressure gradients on the motion of the gas over the entire inner region $x \leq x_p$. We have checked the validity of these two approximations by integrating the resulting equations in the case when a magnetic field is absent altogether, finding that the maximum difference between our computations and the exact results tabulated by Shu (1977) without these approximations to be less than 2% throughout the region $x \leq 0.2$, with the density and flow velocity matching to three significant digits for $x \leq 0.1$.

With the two approximations discussed above, equations (I.34)–(I.38) in a spherical coordinate system (r, θ, φ) read

$$\tau\frac{\partial\alpha}{\partial\tau} + (v-x)\frac{\partial\alpha}{\partial x} + \frac{w}{x}\frac{\partial\alpha}{\partial\theta} - 2\alpha + 2\frac{\alpha v}{x} + \frac{\alpha w}{x}\cot\theta = -\alpha\left(\frac{\partial v}{\partial x} + \frac{1}{x}\frac{\partial w}{\partial\theta}\right), \tag{2}$$

$$\tau\frac{\partial v}{\partial\tau} + (v-x)\frac{\partial v}{\partial x} + \frac{w}{x}\frac{\partial v}{\partial\theta} - \frac{w^2}{x} + \frac{m_0}{x^2} = -\tau^2\frac{\mathscr{F}(\phi)}{\alpha}\frac{\partial\phi}{\partial x}, \tag{3}$$

$$\tau\frac{\partial w}{\partial\tau} + (v-x)\frac{\partial w}{\partial x} + \frac{w}{x}\frac{\partial w}{\partial\theta} + \frac{vw}{x} = -\tau^2\frac{\mathscr{F}(\phi)}{\alpha}\frac{1}{x}\frac{\partial\phi}{\partial\theta}, \tag{4}$$

$$\tau\frac{\partial\phi}{\partial\tau} + (v-x)\frac{\partial\phi}{\partial x} + \frac{w}{x}\frac{\partial\phi}{\partial\theta} + 2\phi = \tau^2\frac{\mathscr{F}(\phi)}{\chi\alpha^{3/2}}\left[\left(\frac{\partial\phi}{\partial x}\right)^2 + \frac{1}{x^2}\left(\frac{\partial\phi}{\partial\theta}\right)^2\right], \tag{5}$$

where

$$\mathscr{F}(\phi) = \frac{1}{x^2\sin^2\theta}\left[\frac{\partial^2\phi}{\partial x^2} + \frac{1}{x^2}\frac{\partial^2\phi}{\partial\theta^2} - \frac{\cot\theta}{x^2}\frac{\partial\phi}{\partial\theta}\right], \tag{6}$$

and we have dropped the subscript n to simplify the notation. The effects of ambipolar diffusion enter in equation (5) only in a factor $1/\chi$. Since the boundary conditions for the overall problem of the collapse of the magnetized singular isothermal sphere can be formulated without introducing any other dimensionless parameters (as long as $\tau \ll 1$; see Appendix A of Paper I), different spacetime solutions for the nondimensional problem are distinguished merely by different values for χ.

For a given choice of $\chi \gg 1$, the strong nonlinearity of the magnetic terms prevents an analytical treatment of the inner problem. We cannot obtain a global semianalytical solution by the method of matched asymptotic expansions, as done, for example, by Terebey, Shu, & Cassen (1984, hereafter TSC) for the corresponding problem of rotating collapse. We adopt instead a "patching" technique, whereby we patch a numerical solution of the inner problem to the semianalytical solution of the intermediate problem by requiring continuity of all physical variables at a somewhat arbitrarily chosen interface $x = x_{ext}$ (see, e.g., Roache 1972 and reference therein). To approximate the spirit of asymptotic "matching," whereby continuity of not only physical variables but of all their derivatives holds in a finite region of overlap (i.e., the limiting *functional forms* of all dependent variables *match* as the limit is taken in either direction), we choose a value $x_{ext} = 0.2$ that is larger than x_p for all τ considered in our calculations ($\tau = 0.2$–0.7). We may then check a posteriori whether the numerical technique gives essentially the same answer as the perturbative technique in the common region of validity, $x_p \leq x \leq 0.2$, which will nearly encompass the entire computational grid for very small values of τ (see below).

In a Lagrangian description of the motion of a fluid element, the radial and tangential displacements satisfy $dr = u_r\,dt$ and $r\,d\theta = u_\theta\,dt$. With $(u_r, u_\theta) \equiv a(v, w)$ and $r \equiv atx$, these relations become $t\,dx + x\,dt = v\,dt$ and $tx\,d\theta = w\,dt$. Since $dt/t = d\tau/\tau$, these results motivate us to introduce an auxiliary "time" variable s to describe motion along a streamline in similarity variables. If we define s so that

$$\frac{d\tau}{ds} \equiv \tau, \tag{7}$$

the "velocity" relations read

$$\frac{dx}{ds} = (v-x), \tag{8}$$

$$\frac{d\theta}{ds} = \frac{v}{x}. \tag{9}$$

The derivative with respect to s of a generic function of τ, x, and θ then is

$$\frac{d}{ds} = \frac{d\tau}{ds}\frac{\partial}{\partial\tau} + \frac{dx}{ds}\frac{\partial}{\partial x} + \frac{d\theta}{ds}\frac{\partial}{\partial\theta} = \tau\frac{\partial}{\partial\tau} + (v-x)\frac{\partial}{\partial} + \frac{w}{x}\frac{\partial}{\partial\theta}. \tag{10}$$

We now may write the system of equations (2)–(5) in the compact forms

$$\frac{d\alpha}{ds} - 2\alpha + 2\frac{\alpha v}{x} + \frac{\alpha w}{x}\cot\theta = -\alpha\left(\frac{\partial v}{\partial x} + \frac{1}{x}\frac{\partial w}{\partial \theta}\right), \quad (11)$$

$$\frac{dv}{ds} + \frac{w^2}{x} + \frac{m_0}{x^2} = -\tau^2\frac{\mathscr{F}(\phi)}{\alpha}\frac{\partial \phi}{\partial x}, \quad (12)$$

$$\frac{dw}{ds} + \frac{vw}{x} = -\tau^2\frac{\mathscr{F}(\phi)}{\alpha}\frac{1}{x}\frac{\partial \phi}{\partial \theta}, \quad (13)$$

$$\frac{d\phi}{ds} + 2\phi = \tau^2\frac{\mathscr{F}(\phi)}{\chi\alpha^{3/2}}\left[\left(\frac{\partial \phi}{\partial x}\right)^2 + \frac{1}{x^2}\left(\frac{\partial \phi}{\partial \theta}\right)^2\right]. \quad (14)$$

Equations (7)–(9) suggest a further simplification in the inner region, where the right-hand sides of equations (8) and (9) are large compared to unity, whereas the right-hand side of equation (7) is a small quantity by hypothesis. In the inner region, the variables x and θ can be considered "fast" and the variable τ "slow" with respect to changes of the "orbit time" s. Thus, we may approximate the slow variable to equal a constant, and replace the solution to equation (7), $\tau = \tau_0 e^s$, with the condition

$$\tau(s) \simeq \tau(s = 0) \equiv \tau_0 \quad (15)$$

for the relevant small range Δs of s near zero.

The approximation (15) represents the physical expectation that any given fluid element takes little time (as measured by Δs) to cross the computational domain of the inner region compared to the evolutionary time scale of the accretion flow (as measured by τ). To good approximation, then, the change of the physical variables attached to any given fluid element along its trajectory in the inner region can be computed as occurring at one instant of the accretion flow. We can follow the full evolutionary problem as a series of quasi-steady calculations where $\tau \simeq \tau_0$ appears only as an external parameter determined by the boundary conditions. To appreciate the power of this approach, note that because Paper I analytically supplies the relevant interface boundary conditions for all $\tau < 1$, we may, if we wish, immediately jump to *any* point of the evolution without having to compute the prior evolutionary phases. Our formulation yields, therefore, an especially appropriate technique for the construction of magnetic collapse models for comparison with astronomical objects observed at a specific epoch in time.

2.2. *The Computational Domain and the Boundary Conditions*

The natural boundaries conditions to impose in a problem of accretion onto a central object come from the outside. For the intermediate problem of Paper I, except for gravitation, they were satisfied by requiring the physical variables to match asymptotically the initial unperturbed state at large radii (more accurately, the inner limit of an outer solution). The proper treatment of Poisson's equation requires the imposition of a boundary condition in the limit as one approaches the origin from outside. Paper I assumed that this outer limit of the inner gravitational potential could be obtained by neglecting all terms other than the monopole of the central object. This approximation will continue to hold even in the inner region proper if we can assume that the amount of material transiently passing through the pseudodisk is small in comparison with that stored in the central protostar and centrifugal disk. Since the former equals $\dot{M} \simeq m^{(0)}(0)a^3/G$ times the crossing time $\propto \Delta s$, whereas the latter equals $\dot{M}$ times the evolutionary time $\propto \tau$, the former will be small in comparison to the latter to the same extent that the quasi-steady assumption holds, $\Delta s/\tau \ll 1$.

As shown before, we may ignore the self-gravity of the gas in the inner accretion flow and the pseudodisk, and take the gravitational potential to be that of a central point of reduced mass $m_0 \simeq 0.975$. Only *external* boundary conditions then remain to be specified at any time step, which we assign as the values of all physical variables obtained on $x = x_{\rm ext}$ from the perturbative solution of Paper I for the intermediate region. We further limit the computational domain of the inner region to be larger than an *internal* circle in the meridional plane of radius $x_{\rm int} = x_{\rm ext}/10 = 0.02$. This choice is dictated by physical as well as computational considerations. As we have already noticed in Paper I, the physical validity of some assumptions at the heart of our method breaks down at very short distances from the central hydrostatic protostar. For example, dust and gas heating by the stellar radiation field (Stahler, Shu, & Taam 1980; Adams & Shu 1986) makes the equation of state deviate badly from the simple isothermal law assumed in Paper I for physical radii interior to $\sim$10–100 AU. This heating has little direct effect on the flow, which occurs hypersonically in such regions, but it could affect the validity of the assumed magnetic coupling in the innermost regions, since column densities in excess of ~ 100 g cm^{-2} in the pseudodisk or centrifugal disk (see below) lead to shielding from galactic cosmic rays, whereas temperatures in excess of $\sim 10^3$ K lead to thermal ionization replacing cosmic rays or natural radioactivity as the dominant mechanism for producing charged particles (Umebayashi 1983; Nakano & Umebayashi 1986a, b).

Another restriction on the spatial extent of the formal calculation comes from our neglecting the rotation of the original cloud core and its effects on the collapse dynamics. The latter includes the generation of toroidal magnetic fields from the initially poloidal field. Indeed, rotation plays a dynamically significant role inside the *centrifugal radius*

$$r_C = 0.058 a\Omega_0^2 t^3 \simeq 7\left(\frac{a}{0.35\ \text{km s}^{-1}}\right)\left(\frac{\Omega_0}{4\times 10^{-14}\ \text{s}^{-1}}\right)^2\left(\frac{t}{10^5\ \text{yr}}\right)^3 \text{AU} \quad (16)$$

(Cassen & Moosman 1981; TSC), as discussed in Paper I (§ 5.3). Only for $r \gg r_C$, can the centrifugal effects arising from an initial rotation of the cloud be safely ignored. Our choice of $x_{\rm int} = 0.02$ generally satisfies the constraints arising from typical cases.

In practice, the choice of the computational domain $0.02 \le x \le 0.2$ provides a sufficient spatial range for studying the gravitational collapse in the inner region where the dynamical effects of magnetic fields dominate the characteristics of the flow and lead to the important phenomenon of the formation of a pseudodisk. To study the dense interiors of the pseudodisk or centrifugal disk, where the complex effects of finite resistivity and reconnection may well become important (see § 4.2), will require a separate calculation. The results of this paper may possibly be viewed in this light as providing the boundary conditions or setting the stage for such an interior calculation.

3. THE NUMERICAL METHOD OF SOLUTION

3.1. *The Integration Scheme*

Assume, for the moment, that the right-hand sides of equations (11)–(14) are *known* functions of x and θ. These equations can be integrated as ODEs, together with the two subsidiary ODEs (8) and (9) defining parametrically the trajectory of the given fluid element. To perform this integration, we need "initial" conditions at $s = 0$ for x, θ, α, v, w, and ϕ. For the trajectory part of this problem, consider an ensemble of fluid elements crossing the outer circle $x = x_{\rm ext}$ in the meridional plane at a given infall time $\tau = \tau_0$. For each polar angle $\theta = \theta_0$ on $x = x_{\rm ext}$, we set the orbit clock at $s = 0$ for convenience. Since the perturbative method retains validity on $x = x_{\rm ext}$, we may take the initial values of α, v, w, and ϕ to be attached to the fluid element with initial coordinates $(x_{\rm ext}, \theta_0)$ to be given by the semianalytical solution presented in Paper I, namely

$$\alpha(s=0) = \alpha^{(0)}(x_{\rm ext}) + \tau^2[\alpha_0^{(2)}(x_{\rm ext})P_0(\theta_0) + \alpha_2^{(2)}(x_{\rm ext})P_2(\theta_0)] , \quad (17)$$

$$v(s=0) = v^{(0)}(x_{\rm ext}) + \tau^2[v_0^{(2)}(x_{\rm ext})P_0(\theta_0) + v_2^{(2)}(x_{\rm ext})P_2(\theta_0)] , \quad (18)$$

$$w(s=0) = \tau^2 w_2^{(2)}(x_{\rm ext}) \frac{dP_2(\theta_0)}{d\theta_0} , \quad (19)$$

$$\phi(s=0) = f^{(0)}(x_{\rm ext}) \sin^2\theta_0 + \tau^2[f_0^{(2)}(x_{\rm ext})P_0(\theta_0) + f_2^{(2)}(x_{\rm ext})P_2(\theta_0)] \sin^2\theta_0 . \quad (20)$$

Equations (11)–(14) plus equations (8)–(9), with τ frozen at τ_0, can be integrated following each element of fluid by "marching" in s. This *Lagrangian* integration has a straightforward implementation provided one knows the values of the right-hand side at any position (x, θ) inside the starting contour. The need for the latter information suggests the possibility of an iterative procedure in which the right-hand sides of equations (11)–(14) are calculated by taking the derivatives with respect to x and θ on an *Eulerian* grid of values of the velocity and the magnetic flux function given by a previous iterate. We can perform this last task since τ is fixed (eq. [15]), so α, v, w, and ϕ are functions of x and θ only.

More precisely, let $\boldsymbol{f}$ indicate the vector of the unknown quantities (α, v, w, ϕ). In principle, a workable iterative procedure could consist of the following steps:

1. We make a first guess for the velocity field and the magnetic flux function, that is, we assign v, w, ϕ and their partial derivatives as functions of x and θ, and we compute the right-hand sides of equations (11)–(14).

2. We then integrate equations (11)–(14), together with equations (8)–(9), for the ensemble of fluid elements lying at $s = 0$ on the external boundary with the initial conditions (17)–(20). The integration terminates at the internal boundary $x = x_{\rm int}$ or just before the equatorial plane $\theta = 90^{\circ -}$, whichever is reaches first by the fluid element under consideration. The values of $\boldsymbol{f}$ obtained along the paths of each fluid element are mapped onto an Eulerian grid in the plane (x, θ), where the right-hand sides of equations (11)–(14) are then computed by finite difference on grid points to second-order accuracy in the grid spacing.

3. With the tabulated right-hand sides, we again integrate equations (11)–(14) and (8)–(9) with the same initial conditions for the same fluid elements as in step 2. The positions (x, θ) reached by the fluid elements will generally fall between the Eulerian grid points; hence the computation of the relevant right-hand sides will need interpolation of the tabulated values. We then map the new values of $\boldsymbol{f}$ along the latest paths of the fluid elements onto the fixed (x, θ) grid. The operations performed so far can be represented schematically by the equation

$$\boldsymbol{f} = D[\boldsymbol{f}] , \quad (21)$$

where D is a differential operator containing the right-hand sides of equations (11)–(14) as inhomogeneous terms.

4. The values of $\boldsymbol{f}$ obtained at steps 2 and 3 are then compared on grid points, with repetition of the steps until we achieve the desired level of convergence.

In practice, the stated procedure requires slight addendums to achieve numerical *stability* and sufficient *accuracy*. Stability can be achieved by the method of "under-relaxation." Instead of straightforwardly taking the value suggested by equation (21) we found it useful to construct the $(n + 1)$-th iterate by taking a linear combination of the provisional value

$$\boldsymbol{f}_{(*)} = D[\boldsymbol{f}_{(n)}] \quad (22)$$

and the nth iterate $\boldsymbol{f}_{(n)}$, viz.,

$$\boldsymbol{f}_{(n+1)} = \xi \boldsymbol{f}_{(*)} + (1 - \xi)\boldsymbol{f}_{(n)} , \quad (23)$$

where ξ is a pure number called the *relaxation parameter*. The parameter ξ allows a gradual introduction and a judicious control at every iteration of the back-reaction introduced by the inhomogeneous terms on the right-hand side of equations (2)–(5) on the dynamics of the flow. Its numerical value can be chosen in many different ways. In our specific problem we allowed ξ to vary with x. By trial-and-error tests we found that choosing ξ as a linear function decreasing with x allows smooth and stable iterative cycles.

Accuracy can be compromised unless we pay careful attention to the two interpolations required for each cycle (step 3): one interpolation of $\boldsymbol{f}$ from a set of sparse points to a grid in (x, θ) and one interpolation of the right-hand sides back from grid points to points along the path of a given fluid element. Fortunately, computer software based on mathematical algorithms elaborated for this purpose has become available in the specialized literature. In our work we have used a method described by Cline & Renka (1984) and Renka & Cline (1984) for the interpolation and the evaluation of the gradient of a function of two variables through a set of scattered data points.

3.2. *Tests of the Numerical Code*

As we have already discussed in Paper I, substantial differences in the general formulation of the problem and/or in the adopted initial and boundary conditions prevent a direct comparison of our numerical results with those published by other authors. Nevertheless, our formulation of the problem naturally suggests two tests of the developed numerical code: (1) the self-similar solution found by Shu (1977) for the collapse of the *nonmagnetic* isothermal singular sphere, and (2) the semianalytical perturbative solution for the *magnetic* collapse described in Paper I.

The first test provides essentially a check of the integration routine for ODEs (a Runge-Kutta scheme with adaptive step-size control from Press et al. 1986) and the validity of the simplifying assumptions used to derive equations (11)–(14). As already discussed in § 2.1, the adopted scheme passes the first

test beautifully. Unfortunately, the first test gives no information on the accuracy of the interpolation and differentiation routines since the right-hand sides of equations (12)–(14) vanish identically in the absence of the magnetic field (when $\tau = G^{1/2}B_0 t/2a = 0$ for any finite value of t).

Fortunately, when $B_0 \neq 0$, the second test can still be performed for values of τ small enough (e.g., $\tau \simeq 0.01$–0.05) that the perturbative solution of Paper I remains approximately valid over the entire computational domain, $0.02 \leq x \leq 0.2$. The second test therefore provides an overall check of the accuracy of the code. On carrying out the second test, we found agreement between the perturbative and the numerical solutions of the order of a few percent for grids containing 50 points in both $\log x$ and θ. In contrast to the situation at lower grid resolution, increasing the number of grid points much beyond 50 does not introduce further improvement in the accuracy of the results because truncation errors begin to generate appreciable numerical noise in the computation of spatial derivatives. The results shown in this paper are obtained with a grid of 50 points logarithmically spaced in x and 50 points linearly spaced in θ. The tables of results given in § 4 include pruning of the dense grid to a sparser one; the interested reader may obtain analogous tabulations on the original dense grid by writing to one of the authors (D. G.).

4. NUMERICAL RESULTS AND EXAMPLES

For the two choices $\chi = 11.3$ and $\chi = \infty$, we computed the density distribution α, velocity fields v and w, and self-consistent magnetic flux function ϕ, at several times in the range $\tau = 0.2$–0.7. The adopted computational domain extends in radius from $x = x_{ext} = 0.2$ to $x = x_{ext}/10 = 0.02$, according to the discussions of § 2.1, and from $\theta = 0$ to $\theta = \pi/2$, assuming reflection symmetry about the midplane $\theta = \pi/2$.

Tables 1, 2, 3, and 4 give the results in the case $\chi = 11.3$ for $\tau = 0.3$, 0.5, and 0.7. Tables 5, 6, 7, and 8 show the corresponding results under the assumption of flux freezing, $\chi = \infty$. The Appendix summarizes the scaling procedures needed to convert the dimensionless results to dimensional ones.

4.1. *The "Pseudodisk"*

To illustrate the utility of the dimensionless tabulations, we consider astronomical application to the "standard case," when the initial magnetic field is $B_0 = 30$ μG, the effective sound speed is $a = 0.35$ km s^{-1}, and the dimensional constants γ, C, and G combine to give the value $\chi = 11.3$ (see the discussion in Paper I). Figures 1*a*–1*c* and 2*a*–2*c* show isodensity contours, velocities, and magnetic fields in a meridional plane at six different times, for this standard model.

TABLE 1

VALUES OF $\alpha(x, \theta)$

	θ									
x	0°	10°	20°	30°	40°	50°	60°	70°	80°	90°−
FOR $\chi = 11.3$ AT $\tau = 0.3$										
0.02.....	1.92(2)	1.44(4)	1.48(2)	1.52(2)	1.57(2)	1.65(2)	1.77(2)	1.90(2)	2.19(2)	3.12(2)
0.04.....	7.04(1)	6.20(1)	6.33(1)	6.53(1)	6.86(1)	7.35(1)	8.11(1)	9.33(1)	1.16(2)	2.07(2)
0.06.....	4.12(1)	3.89(1)	3.97(1)	4.28(1)	4.35(1)	4.71(1)	5.24(1)	6.07(1)	7.49(1)	9.43(1)
0.08.....	2.87(1)	2.84(1)	2.87(1)	2.98(1)	3.16(1)	3.41(1)	3.76(1)	4.20(1)	4.68(1)	5.10(1)
0.10.....	2.18(1)	2.22(1)	2.25(1)	2.37(1)	2.45(1)	2.61(1)	2.82(1)	3.04(1)	3.23(1)	3.38(1)
0.12.....	1.77(1)	1.83(1)	1.84(1)	1.90(1)	1.99(1)	2.10(1)	2.22(1)	2.33(1)	2.43(1)	2.48(1)
0.14.....	1.50(1)	1.53(1)	1.56(1)	1.60(1)	1.67(1)	1.72(1)	1.82(1)	1.88(1)	1.93(1)	1.95(1)
0.16.....	1.30(1)	1.34(1)	1.34(1)	1.38(1)	1.43(1)	1.48(1)	1.52(1)	1.57(1)	1.60(1)	1.62(1)
0.18.....	1.17(1)	1.18(1)	1.20(1)	1.21(1)	1.25(1)	1.28(1)	1.32(1)	1.35(1)	1.37(1)	1.38(1)
0.20.....	1.05(1)	1.06(1)	1.07(1)	1.09(1)	1.12(1)	1.14(1)	1.17(1)	1.19(1)	1.20(1)	1.21(1)
FOR $\chi = 11.3$ AT $\tau = 0.5$										
0.02.....	2.12(2)	1.58(2)	1.59(2)	1.60(2)	1.62(2)	1.63(2)	1.65(2)	1.68(2)	1.74(2)	2.68(2)
0.04.....	7.40(1)	6.17(1)	6.29(1)	6.32(1)	6.47(1)	6.61(1)	6.89(1)	7.32(1)	8.06(1)	1.29(2)
0.06.....	4.07(1)	3.61(1)	3.65(1)	3.70(1)	3.89(1)	4.12(1)	4.44(1)	4.98(1)	5.99(1)	1.11(2)
0.08.....	2.72(1)	2.51(1)	2.52(1)	2.61(1)	2.78(1)	3.02(1)	3.35(1)	3.89(1)	4.99(1)	9.25(1)
0.10.....	2.01(1)	1.92(1)	1.94(1)	2.03(1)	2.18(1)	2.39(1)	2.70(1)	3.17(1)	4.00(1)	4.92(1)
0.12.....	1.58(1)	1.55(1)	1.58(1)	1.67(1)	1.80(1)	1.99(1)	2.24(1)	2.58(1)	2.97(1)	3.18(1)
0.14.....	1.30(1)	1.31(1)	1.34(1)	1.42(1)	1.54(1)	1.66(1)	1.88(1)	2.09(1)	2.27(1)	2.35(1)
0.16.....	1.12(1)	1.13(1)	1.16(1)	1.24(1)	1.34(1)	1.47(1)	1.66(1)	1.73(1)	1.82(1)	1.86(1)
0.18.....	9.84	9.98	1.04(1)	1.10(1)	1.19(1)	1.28(1)	1.38(1)	1.46(1)	1.52(1)	1.54(1)
0.20.....	8.84	8.97	9.35	9.93	1.06(1)	1.14(1)	1.21(1)	1.27(1)	1.31(1)	1.32(1)
FOR $\chi = 11.3$ AT $\tau = 0.7$										
0.02.....	1.72(2)	2.01(2)	2.02(2)	2.04(2)	2.06(2)	2.08(2)	2.10(2)	2.28(2)	3.97(2)	4.03(2)
0.04.....	8.72(1)	7.44(1)	7.66(1)	7.69(1)	7.83(1)	7.98(1)	8.28(1)	8.92(1)	1.02(2)	1.73(2)
0.06.....	4.46(1)	4.02(1)	4.03(1)	4.06(1)	4.28(1)	4.53(1)	4.84(1)	5.29(1)	5.92(1)	9.32(1)
0.08.....	2.79(1)	2.52(1)	2.54(1)	2.64(1)	2.84(1)	3.10(1)	3.41(1)	3.87(1)	4.67(1)	8.92(1)
0.10.....	1.95(1)	1.80(1)	1.81(1)	1.92(1)	2.10(1)	2.33(1)	2.67(1)	3.16(1)	4.12(1)	7.42(1)
0.12.....	1.44(1)	1.35(1)	1.38(1)	1.50(1)	1.68(1)	1.92(1)	2.23(1)	2.70(1)	3.53(1)	4.29(1)
0.14.....	1.10(1)	1.08(1)	1.12(1)	1.24(1)	1.42(1)	1.57(1)	1.92(1)	2.30(1)	2.75(1)	2.95(1)
0.16.....	9.06	8.80	9.35	1.07(1)	1.23(1)	1.43(1)	1.67(1)	1.93(1)	2.15(1)	2.24(1)
0.18.....	7.44	7.50	8.24	9.28	1.09(1)	1.26(1)	1.45(1)	1.62(1)	1.74(1)	1.79(1)
0.20.....	6.34	6.60	7.34	8.47	9.86	1.13(1)	1.27(1)	1.39(1)	1.46(1)	1.49(1)

TABLE 2

VALUES OF $\phi(x, \theta)$

	θ									
x	0°	10°	20°	30°	40°	50°	60°	70°	80°	90°⁻
FOR $\chi = 11.3$ AT $\tau = 0.3$										
0.02.....	0	1.85(−3)	6.84(−3)	1.62(−2)	2.86(−2)	3.82(−2)	5.28(−2)	6.65(−2)	7.26(−2)	1.11(−1)
0.04.....	0	2.71(−3)	1.07(−2)	2.40(−2)	4.45(−2)	6.50(−2)	9.24(−2)	1.23(−1)	1.52(−1)	1.91(−1)
0.06.....	0	3.24(−3)	1.37(−2)	2.90(−2)	5.68(−2)	8.56(−2)	1.21(−1)	1.58(−1)	2.00(−1)	2.40(−1)
0.08.....	0	4.38(−3)	1.68(−2)	3.83(−2)	6.70(−2)	1.03(−1)	1.43(−1)	1.86(−1)	2.28(−1)	2.43(−1)
0.10.....	0	4.78(−3)	1.96(−2)	4.33(−2)	7.64(−2)	1.16(−1)	1.60(−1)	2.03(−1)	2.36(−1)	2.46(−1)
0.12.....	0	5.50(−3)	2.16(−2)	4.82(−2)	8.36(−2)	1.25(−1)	1.70(−1)	2.11(−1)	2.39(−1)	2.49(−1)
0.14.....	0	5.92(−3)	2.35(−2)	5.20(−2)	8.95(−2)	1.35(−1)	1.78(−1)	2.16(−1)	2.43(−1)	2.52(−1)
0.16.....	0	6.34(−3)	2.52(−2)	5.52(−2)	9.42(−2)	1.38(−1)	1.83(−1)	2.21(−1)	2.47(−1)	2.56(−1)
0.18.....	0	6.70(−4)	2.67(−2)	5.80(−2)	9.73(−2)	1.42(−1)	1.87(−1)	2.26(−1)	2.50(−1)	2.60(−1)
0.20.....	0	7.08(−3)	2.78(−2)	6.05(−2)	1.02(−1)	1.48(−1)	1.93(−1)	2.31(−1)	2.56(−1)	2.65(−1)
FOR $\chi = 11.3$ AT $\tau = 0.5$										
0.02.....	0	1.84(−3)	8.14(−3)	2.27(−2)	3.76(−2)	5.22(−2)	6.60(−2)	7.90(−2)	9.05(−2)	1.00(−1)
0.04.....	0	2.32(−3)	9.76(−3)	2.41(−2)	4.39(−2)	6.57(−2)	8.73(−2)	1.08(−1)	1.28(−1)	1.44(−1)
0.06.....	0	2.72(−3)	1.15(−2)	2.74(−2)	4.99(−2)	7.65(−2)	1.05(−1)	1.33(−1)	1.61(−1)	1.87(−1)
0.08.....	0	3.17(−3)	1.31(−2)	3.07(−2)	5.58(−2)	8.65(−2)	1.20(−1)	1.56(−1)	1.92(−1)	2.30(−1)
0.10.....	0	3.57(−3)	1.46(−2)	3.40(−2)	6.16(−2)	9.59(−2)	1.35(−1)	1.76(−1)	2.17(−1)	2.45(−1)
0.12.....	0	3.95(−3)	1.61(−2)	3.62(−2)	6.72(−2)	1.05(−1)	1.47(−1)	1.91(−1)	2.30(−1)	2.48(−1)
0.14.....	0	4.31(−3)	1.75(−2)	4.03(−2)	7.27(−2)	1.13(−1)	1.58(−1)	2.03(−1)	2.38(−1)	2.52(−1)
0.16.....	0	4.68(−3)	1.90(−2)	4.35(−2)	7.80(−2)	1.21(−1)	1.67(−1)	2.11(−1)	2.44(−1)	2.56(−1)
0.18.....	0	5.06(−3)	2.05(−2)	4.67(−2)	8.32(−2)	1.28(−1)	1.75(−1)	2.19(−1)	2.49(−1)	2.60(−1)
0.20.....	0	5.46(−3)	2.20(−2)	5.00(−2)	8.86(−2)	1.34(−1)	1.83(−1)	2.25(−1)	2.55(−1)	2.65(−1)
FOR $\chi = 11.3$ AT $\tau = 0.7$										
0.02.....	0	1.29(−3)	3.83(−3)	8.24(−3)	5.27(−2)	7.46(−2)	6.28(−2)	1.02(−2)	1.50(−1)	1.61(−1)
0.04.....	0	1.39(−3)	4.82(−3)	1.26(−2)	5.59(−2)	8.70(−2)	1.15(−1)	1.42(−1)	1.84(−1)	2.00(−1)
0.06.....	0	1.50(−3)	6.02(−3)	1.57(−2)	5.63(−2)	8.85(−2)	1.20(−1)	1.52(−1)	1.75(−1)	1.87(−1)
0.08.....	0	1.66(−3)	7.27(−3)	1.80(−2)	5.69(−2)	9.05(−2)	1.24(−1)	1.60(−1)	1.90(−1)	1.81(−1)
0.10.....	0	1.93(−3)	8.18(−3)	2.03(−2)	4.77(−2)	9.12(−2)	1.31(−1)	1.69(−1)	2.02(−1)	2.29(−1)
0.12.....	0	2.20(−3)	9.05(−3)	2.28(−2)	5.71(−2)	9.30(−2)	1.33(−1)	1.75(−1)	2.13(−1)	2.48(−1)
0.14.....	0	2.38(−3)	1.17(−2)	2.96(−2)	5.78(−2)	1.01(−1)	1.41(−1)	1.86(−1)	2.29(−1)	2.51(−1)
0.16.....	0	2.68(−3)	1.21(−2)	3.02(−2)	5.98(−2)	1.05(−1)	1.47(−1)	1.96(−1)	2.41(−1)	2.55(−1)
0.18.....	0	2.75(−3)	1.25(−2)	3.18(−2)	6.32(−2)	1.10(−1)	1.52(−1)	2.08(−1)	2.46(−1)	2.60(−1)
0.20.....	0	3.03(−3)	1.35(−2)	3.44(−2)	6.85(−2)	1.15(−1)	1.67(−1)	2.17(−1)	2.53(−1)	2.66(−1)

TABLE 3

VALUES OF $v(x, \theta)$

	θ									
x	0°	10°	20°	30°	40°	50°	60°	70°	80°	90°⁻
FOR $\chi = 11.3$ AT $\tau = 0.3$										
0.02.....	−9.52	−9.50	−9.48	−9.39	−9.26	−8.97	−8.78	−8.41	−7.87	−7.74
0.04.....	−6.51	−6.50	−6.48	−6.45	−6.41	−6.25	−6.21	−6.04	−5.87	−5.80
0.06.....	−5.14	−5.13	−5.12	−5.09	−5.06	−5.01	−4.95	−4.89	−4.82	−5.04
0.08.....	−4.29	−4.28	−4.28	−4.26	−4.23	−4.21	−4.18	−4.16	−4.16	−4.21
0.10.....	−3.69	−3.69	−3.68	−3.66	−3.65	−3.64	−6.63	−3.62	−3.62	−3.61
0.12.....	−3.24	−3.23	−3.22	−3.22	−3.21	−3.19	−3.17	−3.16	−3.16	−3.17
0.14.....	−2.87	−2.87	−2.86	−2.86	−2.84	−2.83	−2.82	−2.80	−2.80	−2.81
0.16.....	−2.57	−2.57	−2.56	−2.56	−2.54	−2.53	−2.52	−2.50	−2.50	−2.50
0.18.....	−2.31	−2.31	−2.30	−2.29	−2.28	−2.28	−2.25	−2.24	−2.24	−2.24
0.20.....	−2.08	−2.08	−2.08	−2.07	−2.05	−2.04	−2.03	−2.02	−2.01	−2.01
FOR $\chi = 11.3$ AT $\tau = 0.5$										
0.02.....	−9.53	−9.53	−9.52	−9.52	−9.31	−9.10	−8.89	−8.41	−7.79	−7.59
0.04.....	−6.53	−6.53	−6.53	−6.53	−6.51	−6.42	−6.25	−5.98	−5.54	−5.11
0.06.....	−5.16	−5.16	−5.15	−5.14	−5.10	−5.05	−4.93	−4.73	−4.45	−4.16
0.08.....	−4.32	−4.31	−4.30	−4.29	−4.26	−4.21	−4.11	−3.97	−3.80	−3.80
0.10.....	−3.73	−3.72	−3.71	−3.69	−3.66	−3.61	−3.54	−3.44	−3.39	−3.52
0.12.....	−3.28	−3.27	−3.26	−3.24	−3.21	−3.16	−3.10	−3.05	−3.04	−3.08
0.14.....	−2.92	−2.91	−2.90	−2.88	−2.84	−2.80	−2.75	−2.72	−2.71	−2.73
0.16.....	−2.62	−2.62	−2.60	−2.58	−2.54	−2.50	−2.46	−2.43	−2.42	−2.43
0.18.....	−2.37	−2.36	−2.34	−2.32	−2.28	−2.25	−2.21	−2.18	−2.17	−2.16
0.20.....	−2.14	−2.14	−2.12	−2.09	−2.06	−2.02	−1.98	−1.96	−1.94	−1.93
FOR $\chi = 11.3$ AT $\tau = 0.7$										
0.02.....	−9.55	−9.59	−9.66	−9.68	−9.42	−9.30	−9.01	−8.56	−6.06	−1.42
0.04.....	−6.56	−6.58	−6.61	−6.72	−6.78	−6.79	−6.69	−6.47	−6.13	−5.48
0.06.....	−5.20	−5.22	−5.23	−5.28	−5.32	−5.27	−5.23	−4.98	−4.54	−3.95
0.08.....	−4.37	−4.36	−4.38	−4.40	−4.41	−4.40	−4.28	−4.07	−3.75	−3.63
0.10.....	−3.78	−3.77	−3.80	−3.78	−3.78	−3.73	−3.62	−3.48	−3.22	−3.34
0.12.....	−3.34	−3.33	−3.33	−3.33	−3.31	−3.23	−3.06	−2.89	−2.84	−3.13
0.14.....	−2.99	−2.98	−2.97	−2.95	−2.90	−2.83	−2.72	−2.62	−2.58	−2.83
0.16.....	−2.70	−2.70	−2.68	−2.65	−2.60	−2.50	−2.40	−2.33	−2.31	−2.53
0.18.....	−2.45	−2.44	−2.41	−2.37	−2.30	−2.24	−2.12	−2.08	−2.06	−2.06
0.20.....	−2.23	−2.22	−2.18	−2.13	−2.06	−1.99	−1.92	−1.87	−1.83	−1.82

TABLE 4

VALUES OF $w(x, \theta)$

	θ									
x	0°	10°	20°	30°	40°	50°	60°	70°	80°	90°⁻
FOR $\chi = 11.3$ AT $\tau = 0.3$										
0.02.....	0	5.31(−1)	1.11	1.79	2.19	3.25	3.70	4.39	4.80	5.20
0.04.....	0	3.39(−1)	6.74(−1)	1.04	1.34	1.75	2.05	2.46	2.64	2.58
0.06.....	0	2.71(−1)	4.87(−1)	7.37(−1)	9.27(−1)	1.18	1.38	1.52	1.46	1.48
0.08.....	0	1.74(−1)	3.77(−1)	5.29(−1)	6.95(−1)	8.22(−1)	9.15(−1)	9.13(−1)	6.52(−1)	0
0.10.....	0	1.51(−1)	2.77(−1)	4.10(−1)	5.05(−1)	5.77(−1)	6.02(−1)	5.35(−1)	3.84(−1)	0
0.12.....	0	1.15(−1)	2.20(−1)	3.06(−1)	3.70(−1)	4.08(−1)	4.00(−1)	3.28(−1)	2.34(−1)	0
0.14.....	0	8.69(−2)	1.69(−1)	2.30(−1)	2.74(−1)	2.92(−1)	2.72(−1)	2.16(−1)	2.13(−1)	0
0.16.....	0	7.10(−2)	1.26(−1)	1.74(−1)	2.04(−1)	2.12(−1)	1.94(−1)	1.49(−1)	1.18(−1)	0
0.18.....	0	4.77(−2)	9.65(−2)	1.34(−1)	1.54(−1)	1.57(−1)	1.41(−1)	1.07(−1)	6.51(−2)	0
0.20.....	0	4.08(−2)	7.67(−2)	1.03(−1)	1.18(−1)	1.18(−1)	1.03(−1)	7.67(−2)	4.08(−2)	0
FOR $\chi = 11.3$ AT $\tau = 0.5$										
0.02.....	0	4.66(−1)	8.48(−1)	1.51	2.20	2.89	3.30	4.03	4.82	5.07
0.04.....	0	2.84(−1)	6.15(−1)	9.53(−1)	1.33	1.70	2.20	2.68	3.33	3.71
0.06.....	0	2.69(−1)	5.46(−1)	7.62(−1)	1.06	1.34	1.71	2.09	2.45	2.68
0.08.....	0	2.35(−1)	4.41(−1)	6.65(−1)	8.64(−1)	1.12	1.37	1.63	1.87	1.79
0.10.....	0	1.86(−1)	3.94(−1)	5.62(−1)	7.52(−1)	9.31(−1)	1.11	1.26	1.24	0
0.12.....	0	1.79(−1)	3.37(−1)	4.98(−1)	6.40(−1)	7.74(−1)	8.86(−1)	9.09(−1)	6.65(−1)	0
0.14.....	0	1.52(−1)	3.03(−1)	4.33(−1)	5.46(−1)	6.39(−1)	6.84(−1)	6.21(−1)	3.82(−1)	0
0.16.....	0	1.37(−1)	2.68(−1)	3.77(−1)	4.65(−1)	5.20(−1)	5.16(−1)	4.25(−1)	2.42(−1)	0
0.18.....	0	1.22(−1)	2.35(−1)	3.29(−1)	3.91(−1)	4.15(−1)	3.86(−1)	2.98(−1)	1.63(−1)	0
0.20.....	0	1.13(−1)	2.13(−1)	2.87(−1)	3.26(−1)	3.27(−1)	2.87(−1)	2.13(−1)	1.13(−1)	0
FOR $\chi = 11.3$ AT $\tau = 0.7$										
0.02.....	0	3.71(−1)	4.96(−1)	1.41	2.05	2.39	3.05	3.64	3.62	1.02
0.04.....	0	1.71(−1)	4.19(−1)	4.55(−1)	8.28(−1)	1.00	1.38	1.71	1.23	1.45
0.06.....	0	1.64(−1)	3.75(−1)	4.46(−1)	6.09(−1)	9.28(−1)	1.25	1.69	1.95	2.21
0.08.....	0	1.95(−1)	3.33(−1)	4.71(−1)	6.59(−1)	9.64(−1)	1.21	1.60	1.90	2.17
0.10.....	0	1.91(−1)	3.27(−1)	4.84(−1)	6.55(−1)	9.43(−1)	1.17	1.46	1.76	1.87
0.12.....	0	1.86(−1)	3.56(−1)	5.03(−1)	6.78(−1)	9.20(−1)	1.10	1.29	1.28	0
0.14.....	0	1.79(−1)	3.60(−1)	5.20(−1)	6.93(−1)	8.83(−1)	9.98(−1)	1.03	7.45(−1)	0
0.16.....	0	1.88(−1)	3.70(−1)	5.42(−1)	6.93(−1)	8.69(−1)	8.59(−1)	7.68(−1)	4.58(−1)	0
0.18.....	0	2.01(−1)	3.93(−1)	5.60(−1)	6.76(−1)	7.43(−1)	7.04(−1)	5.62(−1)	3.06(−1)	0
0.20.....	0	2.22(−1)	4.18(−1)	5.62(−1)	6.40(−1)	6.41(−1)	5.62(−1)	4.18(−1)	2.22(−1)	0

TABLE 5

VALUES OF $\alpha(x, \theta)$

	θ									
x	0°	10°	20°	30°	40°	50°	60°	70°	80°	90°⁻
FOR $\chi = \infty$ AT $\tau = 0.3$										
0.02.....	1.95(2)	1.82(2)	1.77(2)	1.80(2)	1.89(2)	1.98(2)	2.04(2)	2.43(2)	2.88(2)	3.36(2)
0.04.....	8.00(1)	8.04(1)	7.59(1)	7.69(1)	7.73(1)	7.85(1)	8.33(1)	9.36(1)	1.18(2)	2.52(2)
0.06.....	5.12(1)	5.01(1)	5.02(1)	5.04(1)	5.06(1)	5.43(1)	5.29(1)	6.19(1)	7.13(1)	8.72(1)
0.08.....	3.62(1)	3.56(1)	3.50(1)	3.49(1)	3.58(1)	3.69(1)	3.75(1)	3.99(1)	4.28(1)	4.89(1)
0.10.....	2.66(1)	2.63(1)	2.65(1)	2.65(1)	2.65(1)	2.71(1)	2.82(1)	2.95(1)	3.18(1)	3.29(1)
0.12.....	2.09(1)	2.06(1)	2.09(1)	2.10(1)	2.10(1)	2.16(1)	2.22(1)	2.33(1)	2.41(1)	2.46(1)
0.14.....	1.75(1)	1.73(1)	1.73(1)	1.73(1)	1.73(1)	1.77(1)	1.82(1)	1.87(1)	1.92(1)	1.95(1)
0.16.....	1.43(1)	1.43(1)	1.43(1)	1.44(1)	1.46(1)	1.50(1)	1.54(1)	1.57(1)	1.56(1)	1.61(1)
0.18.....	1.21(1)	1.21(1)	1.22(1)	1.24(1)	1.27(1)	1.30(1)	1.33(1)	1.36(1)	1.37(1)	1.39(1)
0.20.....	1.05(1)	1.06(1)	1.07(1)	1.09(1)	1.12(1)	1.14(1)	1.17(1)	1.19(1)	1.20(1)	1.21(1)
FOR $\chi = \infty$ AT $\tau = 0.5$										
0.02.....	2.25(2)	1.74(2)	1.57(2)	1.68(2)	1.81(2)	1.97(2)	2.08(2)	2.18(2)	2.36(2)	2.65(2)
0.04.....	9.75(1)	8.84(1)	7.21(1)	7.42(1)	7.63(1)	8.20(1)	8.96(1)	9.82(1)	1.10(2)	1.54(2)
0.06.....	5.52(1)	5.32(1)	4.64(1)	4.64(1)	4.75(1)	4.79(1)	4.89(1)	6.16(1)	6.82(1)	1.11(2)
0.08.....	3.66(1)	3.42(1)	3.10(1)	3.10(1)	3.28(1)	3.40(1)	3.62(1)	4.03(1)	5.05(1)	7.20(1)
0.10.....	2.51(1)	2.42(1)	2.38(1)	2.39(1)	2.48(1)	2.62(1)	2.85(1)	3.25(1)	4.00(1)	4.42(1)
0.12.....	1.19(1)	1.87(1)	1.84(1)	1.89(1)	1.98(1)	2.12(1)	2.32(1)	2.60(1)	2.95(1)	3.10(1)
0.14.....	1.52(1)	1.49(1)	1.50(1)	1.55(1)	1.64(1)	1.76(1)	1.92(1)	2.10(1)	2.27(1)	2.35(1)
0.16.....	1.22(1)	1.23(1)	1.25(1)	1.31(1)	1.39(1)	1.50(1)	1.62(1)	1.74(1)	1.82(1)	1.87(1)
0.18.....	1.03(1)	1.04(1)	1.07(1)	1.13(1)	1.21(1)	1.31(1)	1.40(1)	1.48(1)	1.54(1)	1.56(1)
0.20.....	8.84	8.97	9.35	9.93	1.06(1)	1.14(1)	1.21(1)	1.27(1)	1.31(1)	1.32(1)
FOR $\chi = \infty$ AT $\tau = 0.7$										
0.02.....	2.55(2)	2.25(2)	1.80(2)	1.84(2)	1.90(2)	2.02(2)	2.13(2)	2.46(2)	2.84(2)	2.92(2)
0.04.....	9.52(1)	9.48(1)	7.69(1)	8.24(1)	8.50(1)	8.65(1)	9.97(1)	1.18(2)	1.51(2)	2.45(2)
0.06.....	5.02(1)	4.51(1)	4.07(1)	4.15(1)	4.58(1)	4.98(1)	5.52(1)	6.63(1)	7.00(1)	1.49(2)
0.08.....	3.33(1)	3.14(1)	2.62(1)	2.97(1)	3.01(1)	3.71(1)	4.21(1)	4.77(1)	5.29(1)	9.64(1)
0.10.....	2.16(1)	2.06(1)	2.08(1)	2.10(1)	2.21(1)	2.91(1)	3.28(1)	3.38(1)	4.91(1)	5.84(1)
0.12.....	1.62(1)	1.55(1)	1.58(1)	1.63(1)	1.75(1)	1.97(1)	2.63(1)	2.98(1)	3.64(1)	3.98(1)
0.14.....	1.23	1.19(1)	1.24(1)	1.24(1)	1.46(1)	1.67(1)	2.14(1)	2.36(1)	2.73(1)	2.92(1)
0.16.....	9.18	9.47	9.92	1.07(1)	1.25(1)	1.46(1)	1.78(1)	1.96(1)	2.13(1)	2.24(1)
0.18.....	7.63	7.71	8.50	9.56	1.12(1)	1.31(1)	1.49(1)	1.66(1)	1.77(1)	1.82(1)
0.20.....	6.34	6.60	7.34	8.47	9.86	1.13(1)	1.27(1)	1.39(1)	1.46(1)	1.49(1)

TABLE 6

VALUES OF $\phi(x, \theta)$

x	θ 0°	10°	20°	30°	40°	50°	60°	70°	80°	90°−
FOR $\chi = \infty$ AT $\tau = 0.3$										
0.02.....	0	3.86(−3)	1.14(−2)	1.89(−2)	2.84(−2)	4.27(−2)	5.83(−2)	7.17(−2)	8.46(−2)	9.67(−1)
0.04.....	0	3.99(−3)	1.37(−2)	3.17(−2)	5.40(−2)	8.01(−2)	1.08(−1)	1.41(−1)	1.75(−1)	2.19(−1)
0.06.....	0	4.46(−3)	1.86(−2)	4.02(−2)	6.87(−2)	1.31(−1)	1.39(−1)	1.78(−1)	2.14(−1)	2.27(−1)
0.08.....	0	5.28(−3)	2.12(−2)	4.60(−2)	7.85(−2)	1.16(−1)	1.57(−1)	1.95(−1)	2.24(−1)	2.42(−1)
0.10.....	0	5.92(−3)	2.31(−2)	5.03(−2)	8.79(−2)	1.26(−1)	1.67(−1)	2.04(−1)	2.33(−1)	2.46(−1)
0.12.....	0	6.34(−3)	2.47(−2)	5.35(−2)	9.06(−2)	1.32(−1)	1.74(−1)	2.12(−1)	2.39(−1)	2.49(−1)
0.14.....	0	6.67(−3)	2.60(−2)	5.63(−2)	9.48(−2)	1.38(−1)	1.80(−1)	2.18(−1)	2.44(−1)	2.53(−1)
0.16.....	0	6.93(−3)	2.70(−2)	5.86(−2)	9.82(−2)	1.43(−1)	1.86(−1)	2.22(−1)	2.48(−1)	2.56(−1)
0.18.....	0	7.19(−3)	2.81(−2)	6.08(−2)	1.02(−1)	1.47(−1)	1.91(−1)	2.28(−1)	2.52(−1)	2.60(−1)
0.20.....	0	7.46(−3)	2.91(−2)	6.28(−2)	1.05(−1)	1.51(−1)	1.95(−1)	2.32(−1)	2.56(−1)	2.65(−1)
FOR $\chi = \infty$ AT $\tau = 0.5$										
0.02.....	0	2.16(−3)	7.96(−3)	1.84(−2)	3.14(−2)	4.45(−2)	5.81(−2)	6.98(−2)	8.02(−2)	8.83(−2)
0.04.....	0	2.69(−3)	1.06(−2)	2.41(−2)	4.22(−2)	6.26(−2)	8.39(−2)	1.05(−1)	1.25(−1)	1.42(−1)
0.06.....	0	3.22(−3)	1.29(−2)	2.92(−2)	5.11(−2)	7.71(−2)	1.05(−1)	1.34(−1)	1.64(−1)	1.91(−1)
0.08.....	0	3.77(−3)	1.50(−2)	3.38(−2)	5.93(−2)	8.99(−2)	1.24(−1)	1.60(−1)	1.98(−1)	2.38(−1)
0.10.....	0	4.28(−3)	1.70(−2)	3.80(−2)	6.67(−2)	1.01(−1)	1.40(−1)	1.81(−1)	2.22(−1)	2.46(−1)
0.12.....	0	4.72(−3)	1.88(−2)	4.21(−2)	7.37(−2)	1.12(−1)	1.54(−1)	1.97(−1)	2.34(−1)	2.49(−1)
0.14.....	0	5.17(−3)	2.06(−2)	4.59(−2)	8.01(−2)	1.21(−1)	1.65(−1)	2.08(−1)	2.40(−1)	2.53(−1)
0.16.....	0	5.61(−3)	2.23(−2)	4.96(−2)	8.62(−2)	1.29(−1)	1.75(−1)	2.16(−1)	2.46(−1)	2.56(−1)
0.18.....	0	6.04(−3)	2.41(−2)	5.33(−2)	9.20(−2)	1.37(−1)	1.83(−1)	2.23(−1)	2.51(−1)	2.59(−1)
0.20.....	0	6.55(−3)	2.58(−2)	5.69(−2)	9.75(−2)	1.44(−1)	1.90(−1)	2.29(−1)	2.56(−1)	2.65(−1)
FOR $\chi = \infty$ AT $\tau = 0.7$										
0.02.....	0	9.60(−4)	5.29(−3)	1.29(−2)	2.81(−2)	3.38(−2)	3.80(−2)	3.81(−2)	5.93(−2)	5.42(−2)
0.04.....	0	1.28(−3)	7.13(−3)	1.76(−2)	3.18(−2)	4.63(−2)	5.67(−2)	7.49(−2)	9.54(−2)	1.31(−1)
0.06.....	0	1.61(−3)	8.31(−3)	1.97(−2)	3.59(−2)	5.54(−2)	7.63(−2)	9.65(−2)	1.24(−1)	1.40(−1)
0.08.....	0	2.14(−3)	9.16(−3)	2.22(−2)	4.08(−2)	6.42(−2)	9.24(−1)	1.22(−1)	1.63(−1)	2.33(−1)
0.10.....	0	2.53(−3)	1.05(−2)	2.51(−2)	5.34(−2)	7.40(−2)	1.09(−1)	1.50(−1)	2.04(−1)	2.45(−1)
0.12.....	0	2.81(−3)	1.19(−2)	2.85(−2)	5.71(−2)	8.64(−1)	1.19(−1)	1.75(−1)	2.27(−1)	2.48(−1)
0.14.....	0	3.26(−3)	1.37(−2)	3.25(−2)	6.09(−2)	9.84(−2)	1.43(−1)	1.94(−1)	2.36(−1)	2.54(−1)
0.16.....	0	3.74(−3)	1.57(−2)	3.72(−2)	6.90(−2)	1.08(−1)	1.58(−1)	2.06(−1)	2.44(−1)	2.56(−1)
0.18.....	0	4.33(−3)	1.82(−2)	3.60(−2)	7.78(−2)	1.22(−1)	1.71(−1)	2.16(−1)	2.49(−1)	2.58(−1)
0.20.....	0	5.14(−3)	2.09(−2)	4.80(−2)	8.60(−2)	1.32(−1)	1.81(−1)	2.25(−1)	2.55(−1)	2.66(−1)

TABLE 7

VALUES OF $v(x, \theta)$

x	θ 0°	10°	20°	30°	40°	50°	60°	70°	80°	90°−
FOR $\chi = \infty$ AT $\tau = 0.3$										
0.02.....	−9.52	−9.51	−9.48	−9.36	−9.22	−8.87	−8.63	−8.30	−8.04	−7.85
0.04.....	−6.51	−6.51	−6.46	−6.42	−6.32	−6.49	−6.39	−6.17	−5.82	−5.74
0.06.....	−5.14	−5.13	−5.12	−5.09	−5.06	−5.06	−4.98	−4.28	−4.64	−4.92
0.08.....	−4.29	−4.28	−4.28	−4.26	−4.24	−4.21	−4.18	−4.17	−4.19	−4.14
0.10.....	−3.69	−3.69	−3.68	−3.67	−3.65	−3.63	−3.62	−3.63	−3.60	−3.56
0.12.....	−3.24	−3.24	−3.23	−3.21	−3.21	−3.18	−3.16	−3.15	−3.16	−3.17
0.14.....	−2.87	−2.87	−2.86	−2.85	−2.84	−2.83	−2.82	−2.80	−2.80	−2.81
0.16.....	−2.57	−2.57	−2.56	−2.55	−2.54	−2.53	−2.51	−2.50	−2.49	−2.50
0.18.....	−2.31	−2.31	−2.30	−2.29	−2.28	−2.27	−2.26	−2.25	−2.24	−2.24
0.20.....	−2.08	−2.08	−2.08	−2.07	−2.05	−2.04	−2.03	−2.02	−2.01	−2.01
FOR $\chi = \infty$ AT $\tau = 0.5$										
0.02.....	−9.53	−9.52	−9.52	−9.40	−9.16	−8.79	−8.45	−8.04	−6.98	−6.55
0.04.....	−6.53	−6.52	−6.51	−6.49	−6.44	−6.32	−6.12	−5.81	−5.34	−4.84
0.06.....	−5.16	−5.16	−5.14	−5.11	−5.07	−4.98	−4.84	−4.64	−4.36	−4.09
0.08.....	−4.32	−4.31	−4.30	−4.27	−4.23	−4.16	−4.06	−3.92	−3.79	−3.97
0.10.....	−3.73	−3.72	−3.71	−3.68	−3.64	−3.58	−3.51	−3.43	−3.42	−3.53
0.12.....	−3.28	−3.27	−3.26	−3.23	−3.19	−3.14	−3.09	−3.05	−3.06	−3.09
0.14.....	−2.92	−2.91	−2.90	−2.87	−2.83	−2.79	−2.76	−2.72	−2.72	−2.74
0.16.....	−2.62	−2.61	−2.60	−2.57	−2.59	−2.50	−2.47	−2.43	−2.43	−2.44
0.18.....	−2.37	−2.36	−2.34	−2.31	−2.28	−2.24	−2.21	−2.18	−2.17	−2.17
0.20.....	−2.14	−2.14	−2.12	−2.09	−2.06	−2.02	−1.99	−1.96	−1.94	−1.93
FOR $\chi = \infty$ AT $\tau = 0.7$										
0.02.....	−9.55	−9.61	−9.48	−9.18	−8.70	−8.08	−7.59	−7.10	−6.10	−5.15
0.04.....	−6.56	−6.58	−6.65	−6.63	−6.47	−5.66	−6.61	−5.71	−5.32	−4.57
0.06.....	−5.20	−5.23	−5.15	−5.21	−5.11	−4.95	−4.85	−4.66	−3.21	−3.97
0.08.....	−4.37	−4.40	−4.34	−4.35	−4.26	−4.12	−4.04	−3.95	−3.91	−3.53
0.10.....	−3.78	−3.79	−3.75	−3.73	−3.68	−3.65	−3.52	−3.53	−3.39	−3.04
0.12.....	−3.34	−3.35	−3.29	−3.27	−3.18	−3.13	−2.90	−2.92	−2.98	−2.83
0.14.....	−2.99	−2.99	−2.95	−2.90	−2.82	−3.05	−2.70	−2.62	−2.63	−2.67
0.16.....	−2.70	−2.70	−2.65	−2.59	−2.53	−2.46	−2.41	−2.34	−2.34	−2.35
0.18.....	−2.45	−2.44	−2.40	−2.35	−2.28	−2.21	−2.15	−2.09	−2.08	−2.07
0.20.....	−2.23	−2.22	−2.18	−2.13	−2.06	−1.99	−1.92	−1.87	−1.83	−1.82

TABLE 8

VALUES OF $w(x, \theta)$

	θ									
x	0°	10°	20°	30°	40°	50°	60°	70°	80°	90°−
FOR $\chi = \infty$ AT $\tau = 0.3$										
0.02.....	0	5.54(−1)	1.65	2.86	4.30	5.53	6.12	7.10	8.04	9.07
0.04.....	0	3.94(−1)	9.59(−1)	1.27	1.72	2.20	2.61	3.33	3.85	3.55
0.06.....	0	3.02(−1)	5.14(−1)	7.50(−1)	1.02	1.28	1.50	1.58	1.30	0
0.08.....	0	1.86(−1)	3.20(−1)	5.02(−1)	6.69(−1)	8.07(−1)	8.79(−1)	8.31(−1)	5.96(−1)	0
0.10.....	0	1.61(−1)	2.34(−1)	3.58(−1)	4.65(−1)	5.38(−1)	5.52(−1)	4.93(−1)	3.29(−1)	0
0.12.....	0	1.21(−1)	1.78(−1)	2.66(−1)	3.36(−1)	3.76(−1)	3.73(−1)	3.14(−1)	1.91(−1)	0
0.14.....	0	9.05(−2)	1.39(−1)	2.00(−1)	2.50(−1)	2.71(−1)	2.60(−1)	2.10(−1)	1.20(−1)	0
0.16.....	0	6.61(−2)	1.11(−1)	1.58(−1)	1.91(−1)	2.02(−1)	1.88(−1)	1.47(−1)	8.11(−2)	0
0.18.....	0	4.79(−2)	9.07(−2)	1.27(−1)	1.48(−1)	1.53(−1)	1.39(−1)	1.05(−1)	5.66(−2)	0
0.20.....	0	4.08(−2)	7.67(−2)	1.03(−1)	1.18(−1)	1.18(−1)	1.03(−1)	7.67(−2)	4.08(−2)	0
FOR $\chi = \infty$ AT $\tau = 0.5$										
0.02.....	0	7.03(−1)	9.64(−1)	1.52	2.45	3.57	3.79	4.13	5.27	5.77
0.04.....	0	4.14(−1)	7.50(−1)	1.05	1.36	1.81	2.29	2.88	3.65	4.42
0.06.....	0	2.75(−1)	5.83(−1)	8.23(−1)	1.11	1.44	1.79	2.19	2.60	2.97
0.08.....	0	2.38(−1)	4.65(−1)	6.93(−1)	9.20(−1)	1.16	1.38	1.56	1.51	0
0.10.....	0	1.91(−1)	3.92(−1)	5.87(−1)	7.66(−1)	9.27(−1)	1.03	1.05	7.97(−1)	0
0.12.....	0	1.82(−1(	3.43(−1)	5.03(−1)	6.40(−1)	7.42(−1)	7.82(−1)	7.08(−1)	4.52(−1)	0
0.14.....	0	1.57(−1)	3.02(−1)	4.34(−1)	5.37(−1)	5.96(−1)	5.90(−1)	4.93(−1)	2.89(−1)	0
0.16.....	0	1.36(−1)	2.66(−1)	3.76(−1)	4.52(−1)	4.83(−1)	4.55(−1)	3.60(−1)	2.01(−1)	0
0.18.....	0	1.23(−1)	2.36(−1)	3.27(−1)	3.83(−1)	3.96(−1)	3.59(−1)	2.73(−1)	1.49(−1)	0
0.20.....	0	1.13(−1)	2.13(−1)	2.87(−1)	3.26(−1)	3.27(−1)	2.87(−1)	2.13(−1)	1.13(−1)	0
FOR $\chi = \infty$ AT $\tau = 0.7$										
0.02.....	0	2.51(−1)	9.25(−1)	1.87	2.69	4.40	4.98	5.77	4.88	6.48
0.04.....	0	1.78(−1)	7.39(−1)	1.16	1.58	2.07	2.55	2.92	3.20	3.32
0.06.....	0	2.51(−1)	6.56(−1)	9.83(−1)	1.28	1.61	1.92	2.15	2.40	2.56
0.08.....	0	2.51(−1)	5.97(−1)	8.60(−1)	1.12	1.37	1.58	1.82	2.17	1.28
0.10.....	0	2.64(−1)	5.46(−1)	7.81(−1)	9.96	1.20	1.33	1.41	1.19	0
0.12.....	0	2.42(−1)	5.07(−1)	7.23(−1)	9.09(−1)	1.06	1.12	1.07	7.16(−1)	0
0.14.....	0	2.37(−1)	4.79(−1)	6.58(−1)	8.32(−1)	9.29(−1)	9.39(−1)	8.08(−1)	4.85(−1)	0
0.16.....	0	2.30(−1)	4.56(−1)	6.34(−1)	7.61(−1)	8.18(−1)	7.82(−1)	6.30(−1)	3.28(−1)	0
0.18.....	0	2.22(−1)	4.35(−1)	5.96(−1)	6.96(−1)	7.22(−1)	6.60(−1)	5.06(−1)	2.78(−1)	0
0.20.....	0	2.22(−1)	4.18(−1)	5.62(−1)	6.40(−1)	6.41(−1)	5.62(−1)	4.18(−1)	2.22(−1)	0

The density profiles in Figures 1*a*–1*c* show that a highly flattened disequilibrium structure forms quite early around the central protostar. With time this pseudodisk expands over radii ranging from $\sim 10^2$ to $\sim 10^3$ AU. As already explained in Paper I, the flattened configuration assumed by the infalling gas is produced by the pinch exerted by the tangential component of the Lorentz force that results from the dragging in of the cloud magnetic field. The Lorentz force deflects ballistically infalling fluid elements entering the computational domain along near radial trajectories toward the equatorial plane until they eventually intersect and shock with their oppositely directed counterparts in the region $r < r_B$ indicated in Figures 1*a*–1*c* by a solid horizontal line. Except for scale, the formation of this structure resembles the mechanism that produces a centrifugal disk during the collapse of a rotating isothermal sphere (Cassen & Moosman 1981; TSC). For example, the inner solution of TSC, obtained under simplifying assumptions similar to those adopted here, shows that fluid elements free-falling under the conservation of specific angular momentum along parabolic streamlines become part of an infinitesimally thin disk upon dissipating their excess energy when they crash into the equatorial plane inside the centrifugal radius r_C. The inability of this thin disk to transfer mass and angular momentum on anything that approaches orbit time scales causes the material in the disk to take on a quasi-equilibrium structure, where outward centrifugal forces very nearly balance the inward pull of the stellar gravity. In contrast, as already pointed out in Paper I, in the presence of realistic amounts of ambipolar diffusion and ohmic dissipation, the pseudodisk cannot support currents large enough to lead to magnetic forces that completely balance the radial force of the stellar gravity. A pseudodisk must constitute a *disequilibrium* structure where gas infalling at supermagnetosonic velocity is deflected toward the central source presumably by a couple of oblique MHD shocks standing back-to-back above and below the equatorial plane.[3] In the interior of the pseudodisk, continued radial inflow at magnetically diluted free-fall speeds should stretch the poloidal fields severely into an ideal configuration (opposed components B_r above and below $\theta = \pi/2$, with the midplane forming a null surface for B_r) for magnetic annihilation and reconnection (see § 4.2).

As a numerical example of the physical conditions above and below the pseudodisk, consider the case $\tau = 0.3$, corresponding to a $M = 0.7\ M_\odot$ protostar. At a distance of 250 AU

[3] Evidence of shocks in the equatorial plane during the collapse of the molecular cloud in the presence of a large-scale magnetic field has been found also by Phillips (1986) in a SPH calculation.

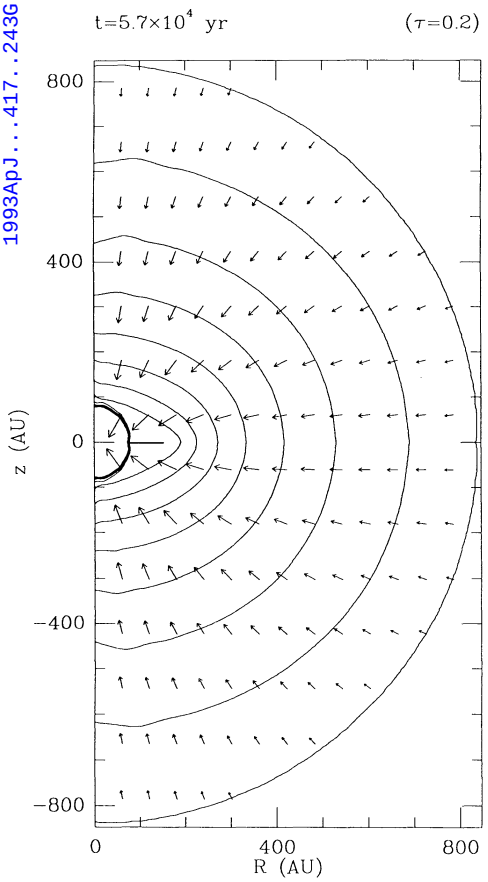

FIG. 1*a*

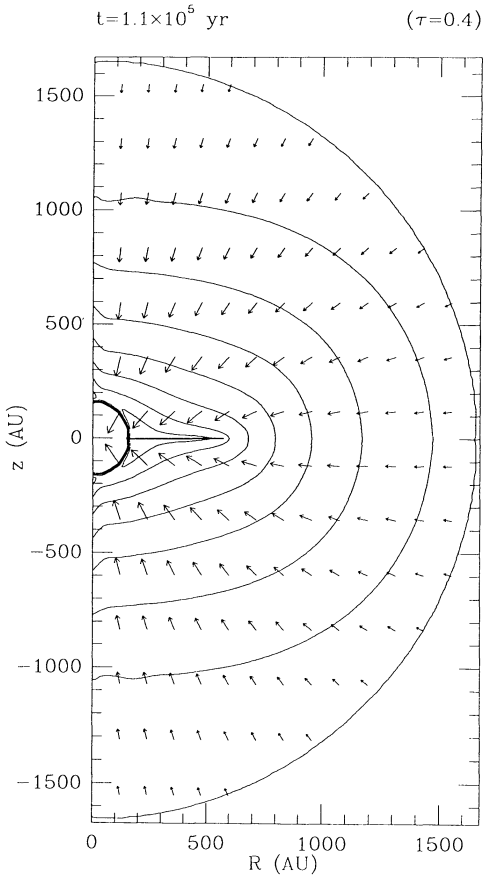

FIG. 1*b*

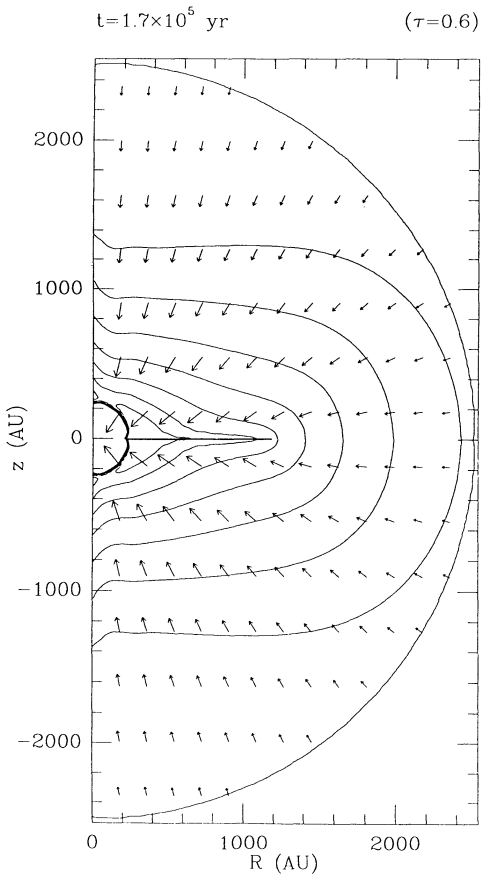

FIG. 1*c*

FIG. 1.—Isodensity contours and velocity field at (*a*) $\tau = 0.2$, (*b*) $\tau = 0.4$, and (*c*) $\tau = 0.6$. Inner and the outer semicircles are the inner and the outer boundaries of the computational domain, respectively. Level contours for the nondimensional density $\alpha = (4\pi G t^2)\rho$ are plotted in all panels starting from $\alpha = 15$, increasing by a factor $2^{1/2}$. Notice that the value of the density in physical units is different in (*a*)–(*c*) for corresponding isodensity contours. Length of the arrows is proportional to the magnitude of the velocity. On the outer boundary of the computational domain the velocity is ~ 2 times the sound speed *a*.

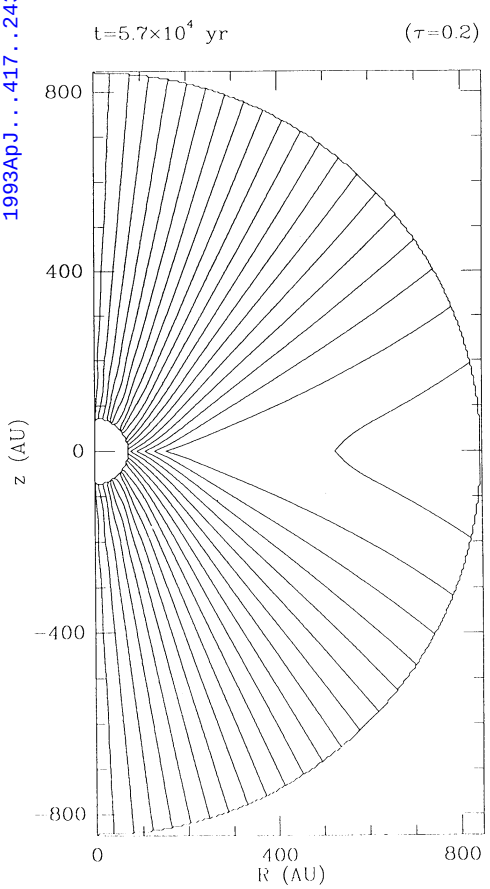

FIG. 2*a*

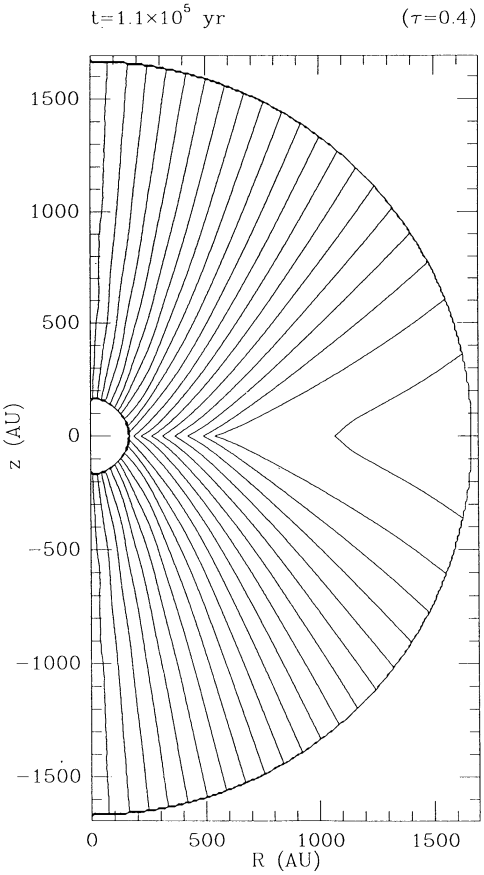

FIG. 2*b*

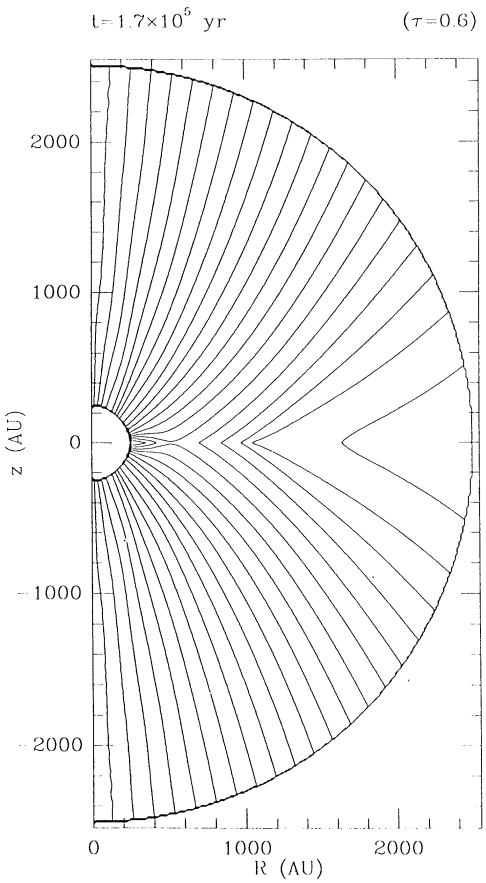

FIG. 2*c*

FIG. 2.—Magnetic field configuration corresponding to the three cases (*a*)–(*c*) presented in Fig. 1. Magnetic field lines are traced as level curves of the nondimensional magnetic flux function $\phi = \Phi/(B_0 a^2 t^2)$, starting from $\phi = 0.01$, increasing as $\phi_j = 0.01\,(j/2 + 1/2)^2$, with $j = 1, 2, \ldots$.

TABLE 9

RADIUS OF THE PSEUDODISK FOR $B_0 = 30$ μG AND $a = 0.35$ km s^{-1}

τ	x_B	t (10^5 yr)	r_B (AU)
0.2.....	0.035	0.57	1.48×10^2
0.3.....	0.055	0.86	3.50×10^2
0.4.....	0.071	1.14	6.02×10^2
0.5.....	0.085	1.43	9.00×10^2
0.6.....	0.094	1.72	1.19×10^3
0.7.....	0.102	2.00	1.47×10^3

from the center, the vertical component of the infall velocity on the pseudodisk is ~ 3 km s^{-1}, the preshock density of the neutrals is $\sim 9 \times 10^6$ cm^{-3}, the magnetic field strength is ~ 1 mG, and the ionization fraction is $\sim 4 \times 10^{-10}$. With these values the magnetosonic velocity in the neutrals is ~ 0.5 km s^{-1}, whereas the magnetosonic velocity in the ions is $\sim 5 \times 10^3$ km s^{-1}. These conditions indicate that the infalling gas must encounter on the equatorial plane a C-shock or a J-shock with a magnetic precursor (Draine 1980). Of course, as the conditions given above vary in both space and time, a detailed analysis is required; in particular, the obliquity of the flow with respect to the magnetic field, as well as the cooling properties of the gas, can play an important role in determining whether the shock will be of the C- or of the J-type (Wardle & Draine 1987). The postshock conditions in the pseudodisk may resemble those thought to be present in some interstellar masers (see, e.g., the review of Reid & Moran 1988).

In Paper I we evaluated the scaling of the radius of the pseudodisk with the physical parameters of the problem, obtaining, in the limit of small time, the dependence expressed by equation (1). Values of r_B determined numerically at six different times are tabulated in Table 9, in nondimensional and physical units, for the standard case. Figure 3 shows the radius of the pseudodisk as function of time in nondimensional units ($x_B = r_B/at$ and $\tau = t/t_m$) for the six cases of Table 9, plotted against the analytical expression derived in Paper I for $\tau \to 0$ ($x_B \propto \tau^{4/3}$, corresponding to $r_B \propto t^{7/3}$). The numerical constant k_B appearing in equation (1) can be evaluated by extrapolating to $t \to 0$ the numerical results, yielding $k_B \simeq 0.12$. For small τ the predicted slope of the x_B versus τ relation is in excellent agreement with the values of x_B computed numerically; for larger τ the analytical power-law expression overestimates the values of x_B: at $\tau = 0.7$ (corresponding to a 2 $M_\odot$ protostar) the relative difference between the analytical and the numerical values of x_B amounts to about 30%.

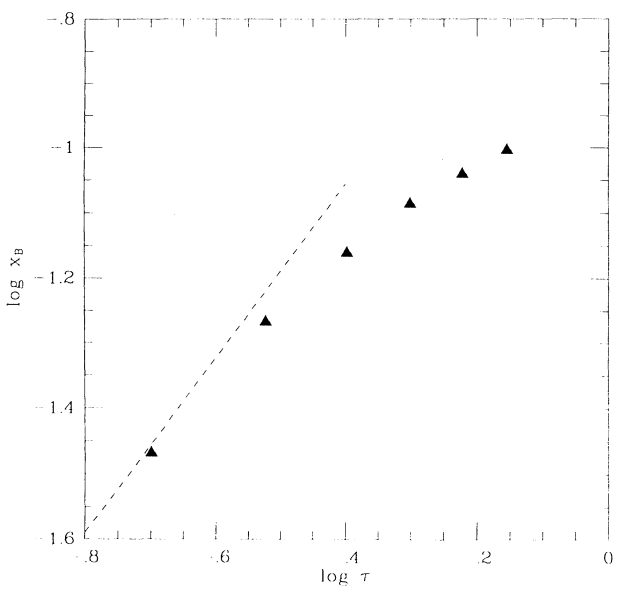

FIG. 3.—Radius of the pseudodisk as a function of time, in nondimensional units ($x_B = r_B/at$, $\tau = t/t_m$). The dashed line is the analytical expression derived in Paper I, valid for $\tau \ll 1$.

In physical units the power-law expression for the radius of the pseudodisk valid for $t \to 0$ reads

$$r_B \simeq 540 \left(\frac{B_0}{30\ \mu\text{G}}\right)^{4/3} \left(\frac{a}{0.35\ \text{km s}^{-1}}\right)^{-1/3} \left(\frac{t}{10^5\ \text{yr}}\right)^{7/3} \text{AU} . \quad (24)$$

Typically, for realistic values of a, B_0, Ω, and t (or mass of the central protostar), $r_B > r_C$, as given by equation (16), by one or two orders of magnitude. We speculate that the characteristic size of an accretion disk resembles r_C during the main infall stage, although viscous evolution can cause the outer edge to spread slowly when the mass infall onto the disk has appreciably slowed or ceased (see, e.g., Cassen & Moosman 1981; Ruden & Pollack 1991). The principal difference introduced by the present considerations, then, involves the idea that protostellar accretion disks are fed equatorially by matter coming through a large pseudodisk in addition to direct infall onto the upper and lower vertical surfaces of the accretion disk. In any case, we are led to the conclusion that for typical conditions of interstellar cloud cores, the density distribution around newly formed stars of mass 0.5–2 $M_\odot$ over scales of a few hundred or a few thousand AU is shaped by gravitational and magnetic (rather than centrifugal) forces. In § 5 we shall speculate on whether such density distributions could be in part responsible for the extended flattened structures revealed around young stars by a variety of observational techniques.

4.2. *The Magnetic Field*

Figures 2*a*–2*c* show the configuration of the magnetic field for the same cases as in Figures 1*a*–1*c*. At early times, the field topology resembles the one found by the semianalytical solution of Paper I. Infalling gas pulls the magnetic field toward the center, with ambipolar diffusion playing a competing but minor role (for $\chi = 11.3 \gg 1$). For comparison, Figures 4*a*–4*b* show the configuration of the magnetic field for $\chi = 11.3$ and $\chi = \infty$ (flux freezing case) at $\tau = 0.7$. Clearly, ambipolar diffusion allows only a relatively modest outward drift of the field lines over the time scale for dynamical collapse, in agreement with the predictions of Nakano and coworkers (Nakano & Umebayashi 1986a, b; Umebayashi & Nakano 1990; Nishi, Nakano, & Umebayashi 1991).

In Figure 2*c* we can discern detachment and reconnection of some field lines across the equatorial plane. No such effect occurs in the frozen-field case presented in Figure 4*b*. In principle, reconnection cannot occur in the absence of true ohmic dissipation, since the diffusion coefficient for ambipolar diffusion alone vanishes on the neighborhood of a null surface for the magnetic field. We conclude that the detachment and reconnection of field lines arise formally from numerical "noise" that keeps the effective diffusion coefficient from disappearing when we evaluate the ambipolar diffusion term in

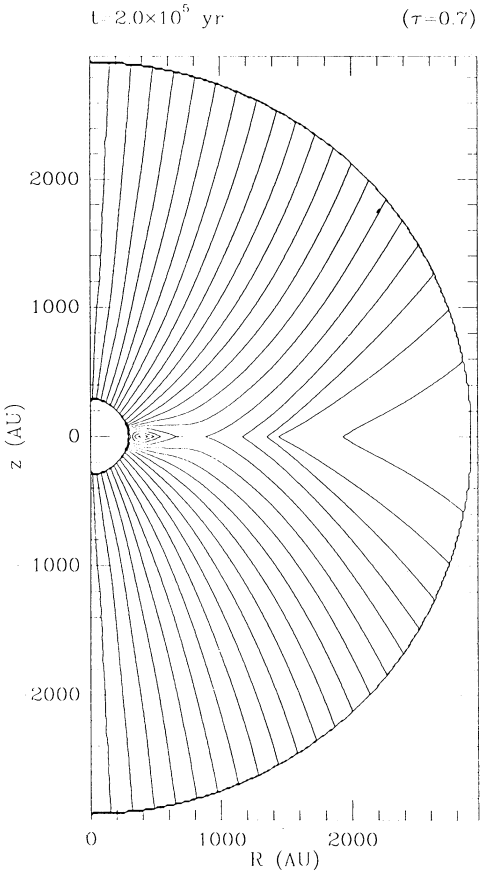

FIG. 4*a*

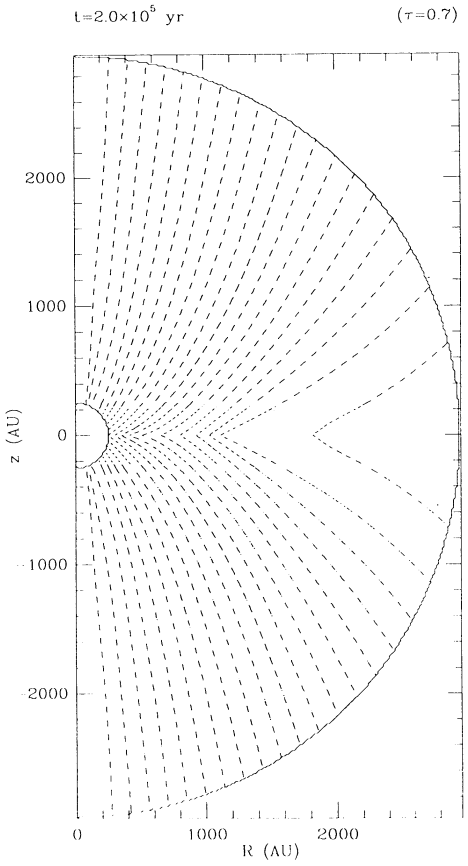

FIG. 4*b*

FIG. 4.—Magnetic field configuration for $\tau = 0.7$ computed with (*a*) $\chi = 11.3$ and (*b*) $\chi = \infty$

the induction equation. Nevertheless, we consider it unwise to regard the changed topology represented by the regions of closed field lines as a purely numerical artifact, since the large shear rates present in the postshock fluid in the pseudodisk may well induce, in the realistic case, a level of turbulent diffusion that is coincidentally being mimicked by the numerical noise of the present calculation. Mestel & Strittmatter (1967) speculated long ago that an analogous change of topology during cloud contraction might occur in the presence of ohmic dissipation, because the strongly pinched configuration of the magnetic field near the equatorial plane is subject to the resistive tearing-mode instability (Furth, Killeen, & Rosenbluth 1963). Moreover, while the ordinary resistive tearing-mode instability allows only the first appearance of a neutral point in the equatorial plane, the global structure of the magnetic field all around a neutral point in the case of a lightly ionized gas is determined by the much stronger ambipolar diffusion (Mestel 1969). Under these circumstances Parker (1963) showed that the process of reconnection of field lines could occur at a rate substantially higher than in the presence of ohmic diffusion alone.

Given the potential important consequences that the process of magnetic reconnection might have on the problems of magnetic flux loss and the transfer of angular momentum within the disk and pseudodisk, we regard a calculation of the detailed structure of the pseudodisk and its magnetic field as a crucial future endeavor. We suspect that such a calculation will show that flux annihilation and reconnection occurs at a rate dictated, not by the magnitude of the dissipative processes, but by the rate at which new flux is brought in via the boundary conditions behind the standing shocks.

5. DISCUSSION AND CONCLUSIONS

Observational evidence for flattened dusty gaseous configurations around young stellar objects (YSOs) have steadily accumulated during the past two decades (see, e.g., Bertout 1989 and Edwards, Ray, & Mundt 1993 for reviews). In most cases, astronomers have attempted to interpret their findings in terms of centrifugally supported accretion disks (Lynden-Bell & Pringle 1974), even though the vertical or radial extents of the structures in some cases exceed theoretical and dynamical expectations by one or two orders of magnitude. This dichotomy led some early researchers (Cantó et al. 1981) to postulate the existence of *two* kinds of YSO disks—circumstellar and interstellar—that differ in their spatial extent and formation mechanisms. At the risk of oversimplification, we resurrect and modify this idea by classifying the available observational evidence into two groups: (1) measurements that suggest the presence of highly flattened structures with radial extents smaller than ~ 100 AU that resemble classical expectations for centrifugally supported disks (e.g., Aumann et al. 1984; Smith &

Terrile 1984; Rucinski 1985; Kenyon & Hartmann 1987; Adams, Emerson, & Fuller 1991; Bertout, Basri, & Bouvier 1988; Strom et al. 1988; Beckwith et al. 1989; Keene & Masson 1990; Plambeck, Wright, & Carlstrom 1990; Car et al. 1993); and (2) measurements that suggest the presence of thicker structures with radial extents of several hundred to a few thousand AU (or material that happens to fall in along the polar regions to smaller radii) that correspond, more likely, to magnetically produced pseudodisks (e.g., Elsasser & Staude 1978; Simon et al. 1985; Sargent & Beckwith 1987, 1991; Bastien & Ménard 1988, 1990; Whitney & Hartmann 1992).

For the present discussion we wish to draw attention to a number of lines of evidence that have proved especially puzzling in the past for an interpretation of all extended structures as simple accretion disks.

1. The presence of unusual mid-infrared emission and absorption features in HL Tau led Cohen (1983) to suggest that the T Tauri star HL Tau must have an associated dust disk. Near-infrared speckle photometry by Beckwith et al. (1984) and direct imaging by Grasdalen et al. (1984) confirmed that HL Tau is surrounded by a radially extended distribution of scattering dust grains. Unfortunately, a conventional accretion disk should generally be too highly flattened to exhibit these effects (see, e.g., Whitney & Hartmann 1992), and Shu, Adams, & Lizano (1987) suggested that HL Tau must be undergoing residual infall (we might now add "in part through a pseudodisk"), a suggestion supported by the near-infrared tomography studies of Beckwith et al. (1989), and by the direct detection of spectroscopic evidence for infall by Grasdalen et al. (1989).

2. The existence of large fractional polarizations in the light from some (angularly unresolved) YSOs led Elsasser & Staude (1978) to propose that these objects must have aspherical distributions of dust around them—flattened enough to produce a polarization signature in the scattering, yet vertically extended enough to extinguish much of the unpolarized light that would otherwise come directly from the central star. Angularly resolved polarization maps of reflection nebulae associated with some YSOs, which show *parallel* polarization vectors near the central source and a *centrosymmetric* pattern at the peripheries, similarly argue against very thin or small disks as the responsible agent (see, e.g., Bastien 1991 for a review). In particular, a flattened distribution of dust, with radial size $\sim 10^3$ AU as deduced from the separation between the "null polarization" points (Bastien & Ménard 1988), is required to produce the parallel vector pattern, either by dichroic extinction by nonspherical grains aligned by a trapped toroidal magnetic field (e.g., Ward-Thompson et al. 1985, Warren-Smith, Draper, & Scarrott 1987), or by multiple scattering on grains in regions of the (pseudo-) disk where the optical depth is ≥ 1 (Bastien & Ménard 1988).

3. Millimeter-wave continuum studies of warm dust around YSOs systematically find structures too small to resolve or barely resolvable ($\sim 10^2$ AU) by the current generation of interferometers, while studies with greater sensitivity by the same telescopes of the emission by molecular gas (CO or CS typically) often find extended structures that span more than 10^3 AU (see, Ohashi et al. 1991, Beckwith & Sargent 1993). We find it tempting to interpret the former as true centrifugal disks, and the latter as pseudodisks that help to feed material into the true disks during the main infall phase of protostellar evolution. This interpretation is consistent with the observational results of Ohashi et al. (1991). These authors notice a strange pattern in their study of infrared sources in the Taurus molecular cloud classified as Class I or II in the scheme of Lada & Wilking (1984) (and interpreted by Adams, Lada, & Shu 1987), respectively, as protostars with infall envelopes or as optically revealed pre–main-sequence stars with surrounding nebular disks). With one exception—L1551, a well-developed bipolar flow source, which may well represent an early transition object—Class I objects exhibit considerable CS line emission from large gaseous structures (presumably pseudodisks), but no detectable continuum-emission from small dust disks. In contrast, with two exceptions—DG Tau and HL Tau, both so-called "flat-spectrum" sources that are difficult to interpret in terms of standard disk models (Adams, Lada, & Shu 1988) and may well be undergoing residual infall (Kenyon, Clavet, & Hartmann 1993)—Class II objects exhibit considerable dust continuum emission from (presumably) unresolved circumstellar disks, but no CS line emission from large extended structures. Ohashi et al. (1991) interpret their observations to indicate that small circumstellar disks are born from the larger extended structures, with the formation of the former coming fairly late in the star formation process. In the main, we would agree with their interpretation, noting, in particular, that equation (16) predicts that the growth of a centrifugal disk to its "full size" is heavily weighted toward late times. Moreover, we would emphasize that in our theory pseudodisks probably represent disequilibrium structures through which the gas flows at magnetically diluted free-fall speeds. Since the typical mass infall rate $\sim a^3/G$ in the Taurus molecular cloud spans 2×10^{-6} to $1 \times 10^{-5}\ M_\odot\ \mathrm{yr}^{-1}$ (Adams et al. 1987), and since the free-fall time across a few thousand AU toward a Sun-like star measures $\sim 10^4$ yr, we expect masses transiently in the pseudodisk to equal ~ 0.02 to $\sim 0.2\ M_\odot$, consistent with the estimates derived from the strength of the CS emission (Ohashi et al. 1991).

In summary, we find the results of Ohashi et al. (1991) especially reassuring to our general picture: namely, sources suspected on the basis of their spectral energy distributions to be undergoing infall (Class I sources), upon close inspection, show evidence for pseudodisks but not well-developed centrifugal disks. Sources suspected on the basis of their spectral energy distributions *not* to be undergoing infall (Class II sources), upon close inspection, show evidence for centrifugal disks but not pseudodisks. Exceptions to these two rules exist but exhibit peculiarities (well-developed outflow in the case of L1551 and flat infrared spectra as well as jets and H-H objects in the cases of DG Tau and HL Tau) that make it plausible that they represent transitional cases.

This work was funded in part by NSF grant AST-9024260 and in part under the auspices of a special NASA Astrophysics Theory Program that supports a joint Center for Star Formation Studies at NASA/Ames Research Center, the University of California at Berkeley, and the University of California at Santa Cruz.

APPENDIX

USE OF THE TABLES

The results of the numerical computation described in this paper are partially presented in Tables 1–8, where the values of the functions $\alpha(x, \theta)$, $\phi(x, \theta)$, $v(x, \theta)$, and $w(x, \theta)$ are tabulated for two cases, $\chi = 11.3$ and $\chi = \infty$, on a 10×10 grid in x and θ at three different times corresponding to $\tau = 0.3$, 0.5, and 0.7. Values of the functions at intermediate times can be computed by interpolation in τ^2; whereas interpolation or extrapolation in $1/\chi$ can provide the values of the functions for different choices of small $1/\chi$. For the convenience of the reader, we recapitulate in this Appendix how to convert the entries in the Tables to physical quantities.

The radial coordinate and time are given by

$$r = \frac{2a^2}{G^{1/2}B_0} x\tau , \qquad t = \frac{2a}{G^{1/2}B_0} \tau ; \tag{25}$$

the densities of neutrals and ions are given by

$$\rho_n = \frac{B_0^2}{16\pi a^2} \frac{\alpha}{\tau^2} , \qquad \rho_i = \frac{CB_0}{4\pi^{1/2}a} \frac{\alpha^{1/2}}{\tau} ; \tag{26}$$

the vector velocities of neutrals and ions are given by

$$\boldsymbol{u}_n = a(v\hat{\boldsymbol{e}}_r + w\hat{\boldsymbol{e}}_\theta) , \qquad \boldsymbol{u}_i = \boldsymbol{u}_n - a\tau^2 \frac{\mathscr{F}(\phi)}{\chi\alpha^{3/2}} \left(\frac{\partial\phi}{\partial x} \hat{\boldsymbol{e}}_r + \frac{1}{x} \frac{\partial\phi}{\partial\theta} \hat{\boldsymbol{e}}_\theta \right) , \tag{27}$$

the magnetic flux is given by

$$\Phi = \frac{4\pi a^4}{GB_0} \tau^2 \phi , \tag{28}$$

and the magnetic field is given by

$$\boldsymbol{B} = B_0 \frac{1}{2x \sin\theta} \left(\frac{1}{x} \frac{\partial\phi}{\partial\theta} \hat{\boldsymbol{e}}_r - \frac{\partial\phi}{\partial x} \hat{\boldsymbol{e}}_\theta \right) , \tag{29}$$

where $\mathscr{F}(\phi)$ is given by equation (6).

For $a = 0.35$ km s^{-1}, $B_0 = 30$ μG, and $C = 3 \times 10^{-17}$ g$^{1/2}$ cm$^{-3/2}$, the constant coefficients in the above equations have the following numerical values:

$$\frac{2a^2}{G^{1/2}B_0} = 3.16 \times 10^{17} \text{ cm} , \qquad \frac{2a}{G^{1/2}B_0} = 9.03 \times 10^{12} \text{ s} , \tag{30}$$

$$\frac{B_0^2}{16\pi a^2} = 1.46 \times 10^{-20} \text{ g cm}^{-3} , \qquad \frac{CB_0}{4\pi^{1/2}a} = 3.63 \times 10^{-27} \text{ g cm}^{-3} , \tag{31}$$

$$\frac{4\pi a^2}{GB_0} = 9.42 \times 10^{30} \text{ Mx} . \tag{32}$$

REFERENCES

Adams, F. C., Emerson, J. P., & Fuller, G. A. 1991, ApJ, 357, 606
Adams, F. C., Lada, C. J., & Shu, F. H. 1987, ApJ, 312, 788
———. 1988, ApJ, 326, 865
Adams, F. C., & Shu, F. H. 1986, ApJ, 308, 836
Aumann, H. H., Gillett, F. C., Beichman, C. A., de Jong, T., Houck, J. R., Low, F. J., & Neugebauer, R. 1984, ApJ, 278, L23
Bastien, P. 1991, in The Physics of Star Formation and Early Stellar Evolution, ed. C. J. Lada & N. D. Kylafis (Dordrecht: Kluwer), 709
Bastien, P., & Ménard, F. 1988, ApJ, 326, 334
———. 1990, ApJ, 364, 232
Beckwith, S. V. W., & Sargent, A. I. 1993, in Protostars and Planets III, ed. M. S. Matthews, & E. Levy (Tucson: Univ. Arizona Press), 521
Beckwith, S. V. W., Sargent, A., Koresko, C. D., & Weintraub, D. A. 1989, ApJ, 343, 393
Beckwith, S. V. W., Zuckerman, B., Skrutski, M. F., & Dyck, H. M. 1984, ApJ, 287, 793
Bertout, C. 1989, ARA&A, 27, 351
Bertout, C., Basri, G., & Bouvier, J. 1988, ApJ, 330, 350
Cantó, J., Rodriguez, L. F., Barral, J. F., & Carral, P. 1981, ApJ, 244, 102
Carr, J., Tokunaga, A. T., Glassgold, A. E., Najita, J., & Shu, F. H. 1993, in preparation
Cassen, P., & Moosman, A. 1981, Icarus, 353
Cline, A. K., & Renka, R. L. 1984, Rocky Mountain J. Math., 14, 119
Cohen, M. 1983, ApJ, 270, L69
Draine, B. T. 1980, ApJ, 241, 1021
Edwards, S., Ray, T., & Mundt, R. 1993, in Protostars and Planets III, ed. M. S. Matthews & E. Levy (Tucson: Univ. Arizona Press), 567
Elsasser, H., & Staude, H. J. 1978, A&A, 70, L3
Furth, H. P., Killeen, J., & Rosenbluth, M. N. 1963, Phys. Fluids, 6, 459
Galli, D., & Shu, F. H. 1993, ApJ, 417, 220
Grasdalen, G. L., Sloane, G., Stout, N., Strom, S. E., & Welty, A. D. 1989, ApJ, 339, L37
Grasdalen, G. L., Strom, S. E., Strom, K. E., Capps, R. W., DeAnne, T., & Castelaz, M. 1984, ApJ, 283, L57
Keene, J., & Masson, C. 1990, ApJ, 355, 635
Kenyon, S. J., & Hartmann, L. 1987, ApJ, 323, 714
Kenyon, S. J., Calvet, N., & Hartmann, L. 1993, ApJ, in press
Lada, C. J., & Wilking, B. A. 1984, ApJ, 287, 610
Lynden-Bell, D., & Pringle, J. E. 1974, MNRAS, 157, 1
Mestel, L. 1969, in Plasma Instabilities in Astrophysics, ed. D. A. Tidman & D. G. Wentzel (New York: Gordon & Breach), 329
Mestel, L., & Strittmatter, P. A. 1967, MNRAS, 137, 95
Nakano, T., & Umebayashi, T. 1986a, MNRAS, 218, 663
———. 1986b, MNRAS, 221, 319
Nishi, R., Nakano, T., & Umebayashi, T. 1991, ApJ, 368, 181
Ohashi, N., Kawabe, R., Hayashi, M., & Ishiguro, M. 1991, AJ, 102, 2054

Parker, E. N. 1963, ApJS, 77, 177
Phillips, G. J. 1986, MNRAS, 211, 571
Plambeck, R. L., Wright, M. C. H., & Carlstrom, J. E. 1990, ApJ, 348, L65
Press, W. H., Flannery, B. P., Teukolsky, S. A., & Vetterling, W. T. 1986, Numerical Recipes (Cambridge Univ. Press)
Reid, M. J., & Moran, J. M. 1988, in Galactic and Extragalactic Radio Astronomy, ed. G. L. Vershuur & K. I. Kellerman (New York: Springer), chap. 6
Renka, R. L., & Cline, A. K. 1984, Rocky Mountain J. Math., 14, 223
Roache, P. J. 1972, Computational Fluid Dynamics (Albuquerque: Hermosa Publ.)
Rucinski, S. M. 1985, AJ, 90, 2321
Ruden, S. P., & Pollack, J. B. 1991, ApJ, 375, 740
Sargent, A. I., & Beckwith, S. V. W. 1987, ApJ, 323, 294
———. 1991, ApJ, 382, L31
Shu, F. H. 1977, ApJ, 214, 488
Shu, F. H., Adams, F. C., & Lizano, S. 1987, ARA&A, 25, 23
Simon, M., Peterson, D. M., Longmore, A. J., Storey, J. W. V., & Tokunaga, A. T. 1985, ApJ, 298, 328
Smith, B. A., & Terrile, R. J. 1984, Science, 226, 1421
Stahler, S. W., Shu, F. H., & Taam, R. E. 1980, ApJ, 241, 637
Strom, K. M., Strom, S. E., Kenyon, S. J., & Hartmann, L. 1988, AJ, 95, 534
Terebey, S., Shu, F. H., & Cassen, P. 1984, ApJ, 286, 529 (TSC)
Umebayashi, T. 1983, Progr. Theory. Phys., 69, 480
Umebayashi, T., & Nakano, T. 1990, MNRAS, 243, 103
Wardle, M., & Draine, B. T. 1987, ApJ, 321, 321
Ward-Thompson, D., Warren-Smith, R. F., Scarrott, S. M., & Wolstencroft, R. D. 1985, MNRAS, 215, 537
Warren-Smith, R. F., Draper, P. W., & Scarrot, S. M. 1987, MNRAS, 227, 749
Whitney, B. A., & Hartmann, L. 1992, 395, 529

Note added in proof.—Recent observations of the ^{13}CO emission in HL Tau by the millimeter array at Nobeyama Observatory (M. Hayashi 1993, personal communication) reveal that the velocity gradients in the flattened 2000 AU structure associated with this source mostly lie along the minor axis rather than along the major axis, consistent with the velocity field (magnetically diluted free fall) of a pseudodisk rather than with that (Keplerian rotation) of a centrifugally supported disk.